Article

Promoting active site renewal in heterogeneous olefin metathesis catalysts

https://doi.org/10.1038/s41586-023-05897-w

Received: 16 December 2021

Accepted: 28 February 2023

Published online: 17 May 2023

Check for updates

Terry Z. H. Gani[1,2], Zachariah J. Berkson[2], Ran Zhu[1], Jong Hun Kang[1], John R. Di Iorio[1], Ka Wing Chan[2], Daniel F. Consoli[1], Sohel K. Shaikh[3], Christophe Copéret[2]✉ & Yuriy Román-Leshkov[1]✉

As an atom-efficient strategy for the large-scale interconversion of olefins, heterogeneously catalysed olefin metathesis sees commercial applications in the petrochemical, polymer and speciality chemical industries[1]. Notably, the thermoneutral and highly selective cross-metathesis of ethylene and 2-butenes[1] offers an appealing route for the on-purpose production of propylene to address the C_3 shortfall caused by using shale gas as a feedstock in steam crackers[2,3]. However, key mechanistic details have remained ambiguous for decades, hindering process development and adversely affecting economic viability[4] relative to other propylene production technologies[2,5]. Here, from rigorous kinetic measurements and spectroscopic studies of propylene metathesis over model and industrial WO_x/SiO_2 catalysts, we identify a hitherto unknown dynamic site renewal and decay cycle, mediated by proton transfers involving proximal Brønsted acidic OH groups, which operates concurrently with the classical Chauvin cycle. We show how this cycle can be manipulated using small quantities of promoter olefins to drastically increase steady-state propylene metathesis rates by up to 30-fold at 250 °C with negligible promoter consumption. The increase in activity and considerable reduction of operating temperature requirements were also observed on MoO_x/SiO_2 catalysts, showing that this strategy is possibly applicable to other reactions and can address major roadblocks associated with industrial metathesis processes.

As with all heterogeneous metathesis catalysts, WO_x/SiO_2 lacks the alkylidene moieties that are responsible for catalytic activity in homogeneous metathesis catalysts[6,7]. Rather, the active sites are thought to form in situ from metal-dioxo precursors on reaction with the olefin substrate at high temperatures[8–11]. The kinetically and thermodynamically demanding nature of this activation process[8,10] results in very few catalytically active metal centres, explaining the low specific reaction rate and high operating temperature requirement of WO_x/SiO_2, as well as the failure to spectroscopically characterize reaction intermediates[9,12]. Indeed, reductive treatments that promote alkylidene formation[12–14] generate active catalysts that operate at low temperatures (for example, 70 °C), but these materials deactivate rapidly for reasons that remain obscure. Furthermore, propylene self-metathesis reaction orders ranging from 0.8 to 1.8 have been reported[10,15,16] despite the well-known Chauvin mechanism[6] predicting a reaction order less than one. These, among other puzzling observations, are symptomatic of broader gaps in the understanding of heterogeneous olefin metathesis that have hindered process development. Our new mechanistic picture for heterogeneous olefin metathesis not only reconciles these longstanding issues, but also shows a strategy for enhancing the activity and reducing the operating temperature requirement of tungsten- and molybdenum-based metathesis catalysts (Fig. 1).

We performed the kinetic studies under differential conditions and in the absence of mass transfer limitations (see Methods and Extended Data Table 2 for details). Using propylene self-metathesis into ethylene and 2-butene as our primary probe reaction, we systematically varied the reactor temperature and propylene concentration (300–330 °C, 20–50 mol% propylene, Fig. 2a,b) while measuring product distributions in the reactor effluent. To avoid the potential confounding effects of metal clusters or interface sites present in classical wet-impregnation catalysts[9], we used a catalyst prepared by the surface organometallic chemistry and thermolytic molecular precursor approach (SOMC–TMP)[17] consisting solely of isolated W(VI)-oxo surface sites supported on silica[12] (3%SOMC) (Extended Data Fig. 1a–c). The presence of isolated W(VI)-oxo surface sites in materials prepared by both approaches (SOMC–TMP and impregnation) allows our conclusions to be broadly generalizable (Extended Data Figs. 1b–e and 2). We measured a propylene reaction order of 1.9 on 3%SOMC (Fig. 2a, orange), confirming the existence of abnormally high reaction orders inherent to isolated tungsten sites. The measured apparent activation energy of 156 kJ mol^{-1} on 3%SOMC (Fig. 2b, orange) is consistent with literature values for supported tungsten catalysts[10,15], but notably higher than those computed for tungsten alkylidene complexes (roughly 80–120 kJ mol^{-1})[18], further hinting at the existence of other kinetically relevant steps beyond the Chauvin cycle.

[1]Department of Chemical Engineering, Massachusetts Institute of Technology (MIT), Cambridge, MA, USA. [2]Department of Chemistry and Applied Biosciences, ETH Zurich, Zurich, Switzerland. [3]Research & Development Center, Saudi Aramco, Dhahran, Saudi Arabia. ✉e-mail: ccoperet@ethz.ch; yroman@mit.edu

Analysis of transient kinetic behaviour provides clues as to the nature of these additional steps. As observed early on for classical supported WO_x catalysts[19], the initial approach to steady state for 3%SOMC was marked by an extended induction period of roughly 24–48 h (Extended Data Fig. 3a) attributable to slow olefin- and silanol-mediated[8] reduction of W(VI)-dioxo sites to W(IV)-oxo sites[8,10,12]. A helium purge of the system at steady state led to a second, shorter, induction period of roughly 1–2 h to return to the original steady-state rate (Extended Data Fig. 3b), suggesting that the active sites are unstable in the absence of propylene, presumably decaying into an inactive resting (off-cycle) state, and are regenerated on re-exposure to propylene. A similar response time resulted from a step change in temperature (Extended Data Fig. 3c). We thus surmised that the steady-state active site fraction varies with reaction conditions because of dynamic site decay and renewal. Indeed, second-order kinetics can be recovered by assuming the fraction of active sites is proportional to the propylene partial pressure, as might be expected from combining first-order metathesis with first-order site renewal and zero-order site decay steps (Extended Data Fig. 4).

The existence of a distinct site decay and renewal cycle operating in parallel to the Chauvin cycle holds important mechanistic implications. If site renewal and metathesis are separate processes, then the olefins used to regenerate the active sites need not be the same olefins that undergo metathesis. Such asymmetry between the ability of the olefin to participate in active site generation or in the metathesis reaction is observed in ethylene and 2-butene cross-metathesis, which shows the same greater-than-first-order behaviour as its reverse reaction (that is, propylene self-metathesis), but with an ethylene order of 0.7 and a 2-butene order of 1.0 (Extended Data Fig. 5a). This difference in reaction orders between the two reactants cannot be explained by differences in their metathesis reactivity, but is instead consistent with 2-butene being more efficient than ethylene at active site renewal to the extent that it becomes responsible for maintaining active sites in the nominally equimolar cross-metathesis system.

The further realization that site renewal and decay rates contribute to the steady-state metathesis rate provides a new handle to improve catalyst efficiency that is orthogonal to traditional catalyst design efforts. In particular, co-feeding an olefin more adept at regenerating or preserving sites than the reactant(s) should improve steady-state catalyst performance by increasing the steady-state population of active sites. A striking example of this phenomenon is the paradoxical increase (by 1.5×) in steady-state propylene self-metathesis rate on addition of 2-butene to the feed (Extended Data Fig. 5b), which runs counter to the expectation that degenerate 2-butene self-metathesis should instead inhibit the reaction by competing for active sites. However, this observation is in fact consistent with 2-butene participating in kinetically relevant site renewal without altering Chauvin cycle intermediates.

The practical feasibility of this promotion strategy hinges on the discovery of a promoter olefin that is not only highly active for site renewal, but also selective against deleterious side reactions forming by-products that would complicate downstream separation. Indeed, promotion of propylene metathesis was first observed in the 1970s (ref. 20), but the polyene promoters investigated then decomposed under reaction conditions. To this end, we screened a set of 1,1-disubstituted olefins that do not readily undergo cross-metathesis[21] for their ability to promote propylene metathesis. All olefins tested increased steady-state propylene metathesis rates by varying degrees, confirming the generality of our promotion strategy (Fig. 1, bottom). A 1.5 mol% concentration of the best-performing promoter, 2,3-dimethyl-1-butene (i4ME), increased steady-state propylene metathesis rates by nearly fivefold at 330 °C and 30-fold at 250 °C (Fig. 2c). The formation of unwanted side products, including isobutene, 2-methyl-2-butene (3ME) and unidentified C7 and C8 hydrocarbons, was minimal, with a less than 1% selectivity relative to the formation rates of metathesis products at 250 °C (Extended Data Table 1a). Despite facile interconversion of i4ME and its positional isomer 4ME (2,3-dimethyl-2-butene) under reaction conditions (Extended Data Table 1b), 4ME is also a competent promoter and we expect a steady-state intermediate promotion factor would be attained if the promoter is continuously separated and recycled, as would be expected in an industrial process.

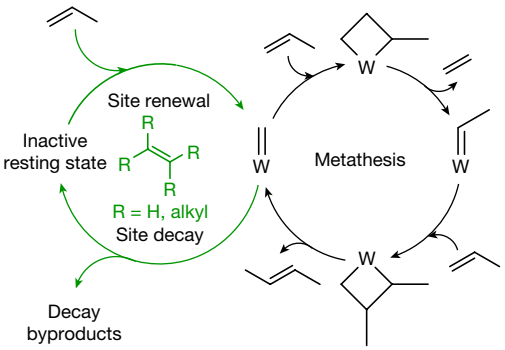

Promoter (mol%)	Promotion factor
2-butene (20%)	1.5 (330 °C)
Isobutene (20%)	2.5 (330 °C)
4ME (1.5%)	3.8 (330 °C)
i4ME (1.5%)	4.6 (330 °C)
i4ME (1.5%)	30 (250 °C)

Fig. 1 | Promotion of heterogeneous olefin metathesis by manipulating site renewal and decay. Top, schematic illustrating the relationship between steady-state Chauvin cycle metathesis and promoter-controlled site renewal and/or site decay. W represents a silica-supported mononuclear tungsten active site where the support has been omitted for clarity. Bottom, the promotional effect of various co-fed olefins on propylene metathesis rates. 4ME, 2,3-dimethyl-2-butene; i4ME, 2,3-dimethyl-1-butene. The promotion factor is defined as the steady-state product formation rate in the presence of promoter divided by the steady-state product formation rate without promoter. Methods of promoter introduction and full experimental details are provided in the Methods. Reaction conditions were: 10 mg 3%SOMC pretreated at 550 °C under 100 ml min^{-1} He for 1 h, 50 ml min^{-1} total gas flow rate (50% C_3H_6 with balance He), WHSV = 0.0019 mol C_3H_6 per g_{cat} s^{-1}.

We performed a series of mechanistic studies to probe the pathways of active site renewal and decay and explain how promoter olefins alter this balance. First, the reaction rate reverts to its original steady-state value on stopping promoter flow (Fig. 2c), confirming that the promoter does not irreversibly alter active sites. Next, observation of temporary promotion on exposure of a purged catalyst to 4ME (Extended Data Fig. 6a) confirms that adsorbed promoter molecules, rather than gas-phase promoter molecules, are responsible for the promotional effect. Kinetic studies performed in the presence of promoter molecules further show that co-feeding 1.0 mol% 4ME + 0.5 mol% i4ME decreases the propylene reaction order from 1.9 to 0.7 at 330 °C (Fig. 2a), accompanied by a combined promoter reaction order of 0.8 (Extended Data Fig. 6b), in which the use of a 4ME and i4ME mixture instead of a pure-component promoter feed minimizes undue variability that would arise from the approach to equilibrium at reaction conditions (Extended Data Table 1b). Consistent with our kinetic analysis (Methods), this result indicates that the promoter reduces the dependence of the active site fraction on propylene concentration. The promoter also decreases the apparent activation energy by 40 to 119 kJ mol^{-1} (Fig. 2b), rationalizing the notable increase in promotion factor at lower temperatures (lower than 300 °C).

We then used in situ diffuse reflectance infrared Fourier transform spectroscopy (DRIFTS) to better understand how olefinic substrates and promoters interact with the catalyst surface. Exposure of spent

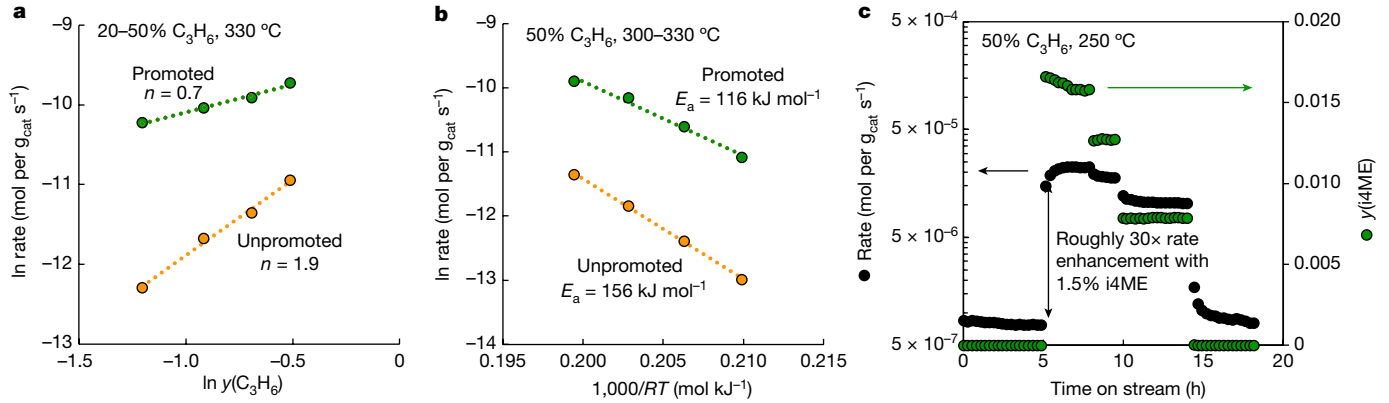

Fig. 2 | Effect of co-fed promoters on propylene metathesis activity and kinetics. a, Reaction order plots of propylene metathesis without promoter (orange) and with promoter (1.0 mol% 4ME + 0.5 mol% i4ME, green). **b**, Arrhenius plots of propylene metathesis without promoter (orange) and with promoter (1.0 mol% 4ME + 0.5 mol% i4ME, green). **c**, Effect of promoter cycling on metathesis activity. R is the gas constant in J mol^{-1} K^{-1} and T is temperature in K. Reaction conditions were: 10 mg 3%SOMC pretreated at 550 °C under 100 ml min^{-1} He for 1 h, 50 ml min^{-1} total gas flow rate (propylene + balance He or He saturated with promoter; propylene concentration and temperature are indicated in each subplot). Full experimental details are provided in the Methods.

3%SOMC to propylene at 50 °C, followed by purging of gas-phase and physisorbed hydrocarbons, yielded a broad series of peaks in the sp^3 C–H stretching region (Fig. 3a). On the basis of: (1) comparison of the relative peak intensities to those of chemisorbed isopropoxy species reported in previous studies[8], (2) the absence of peaks in the sp^2 C–H region and C=O regions that precludes other plausible assignments such as π complexes or acetone, (3) the presence of strong Brønsted acid sites as directly confirmed by solid-state nuclear magnetic resonance (NMR) analysis of the precatalysts treated with ^{15}N-labelled pyridine (Extended Data Fig. 6c) and (4) the reversibility and exothermicity of the adsorption process, as demonstrated by rapid decay of DRIFTS signals on heating under N_2 (Extended Data Fig. 6d), we assign these peaks to chemisorbed alkoxy species probably created by a Brønsted acid–base reaction involving propylene and a silanol group with increased acidity induced by a proximal tungsten site[22,23]. In the absence of W-oxo species, free surface silanol groups are insufficiently acidic to chemisorb propylene in this manner (Extended Data Fig. 6e,f). Propylene exposure at 350 °C resulted in a virtually identical spectrum to that obtained from exposure at 50 °C, suggesting that isopropoxy formation remains the dominant catalyst–substrate interaction under reaction conditions (Extended Data Fig. 6g,h). Chemisorption of other olefins yielded absorption bands in the same region also attributable

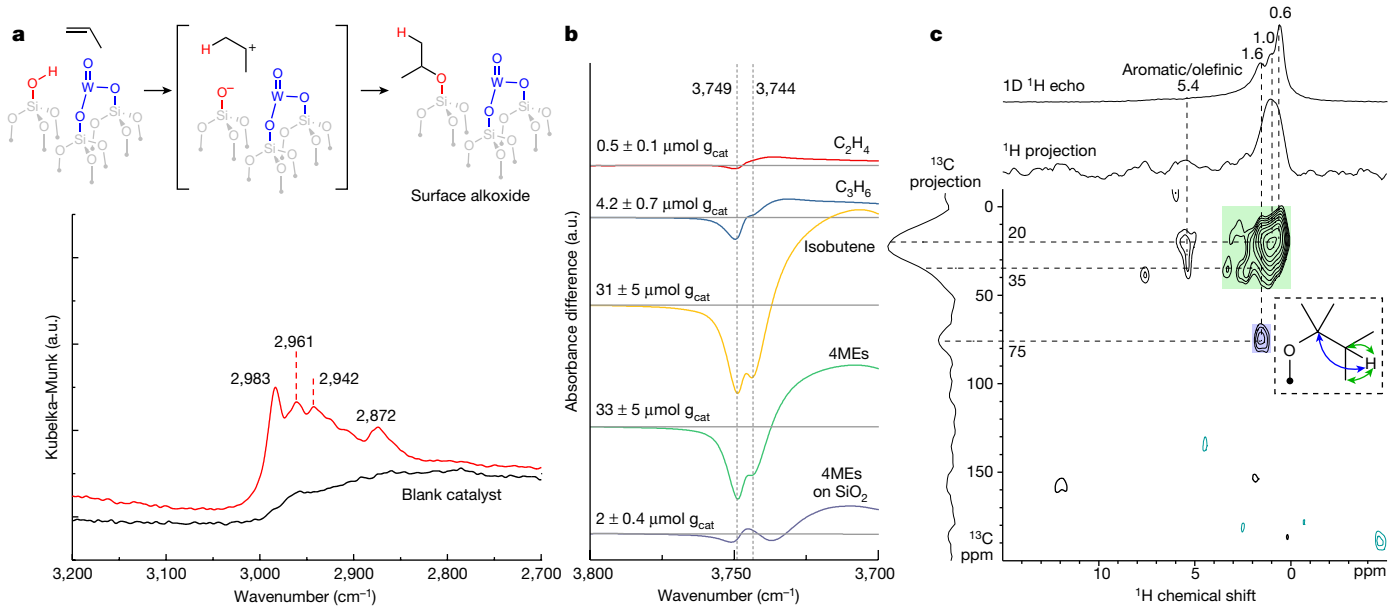

Fig. 3 | Infrared and solid-state NMR studies of olefin chemisorption on spent catalyst. a, DRIFTS spectrum of propylene chemisorbed on spent 3%SOMC at 50 °C. The formation of surface alkoxide species proposed to be responsible for the observed peaks is illustrated above. **b**, FTIR spectra showing absorbance differences in the Si–OH region relative to pretreated samples at 50 °C for different chemisorbed olefins. a.u., arbitrary units. **c**, Solid-state 2D ^{1}H{^{13}C} D-HMQC NMR correlation spectrum of spent catalyst contacted with propylene and i4ME. The spectrum was acquired at 9.4 T, 298 K, 40 kHz MAS, and with dipolar recoupling periods of 60 rotor periods (1.5 ms). The 1D ^{13}C or ^{1}H projections of the 2D spectrum are shown along the ordinate and abscissa, respectively, and a 1D ^{1}H echo spectrum acquired under the same conditions is shown for comparison. Although the exact structure of the surface alkoxide cannot be identified from solid-state NMR alone due to the possibility of skeletal isomerization, the schematic inset shows ^{1}H–^{13}C interactions for a structure that is consistent with the observed correlated signal intensities (green and blue shaded regions). Full sample preparation and measurement details are provided in the Methods.

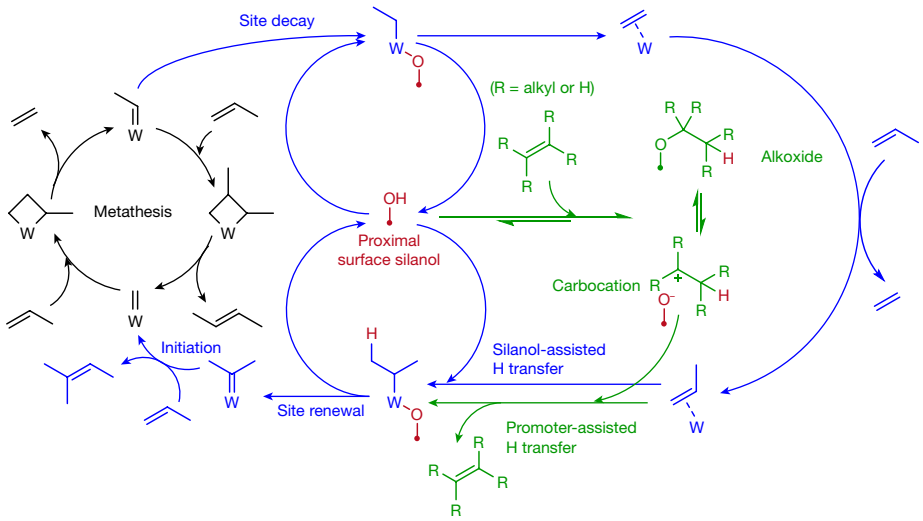

Fig. 4 | Proposed mechanisms for site renewal, site decay and promotion. Proposed catalytic cycle integrating metathesis with in situ silanol-catalysed site renewal and decay and promoter-assisted proton transfer. The colours and labels are as discussed in the main text. W represents a silica-supported mononuclear tungsten active site at which the support has been omitted for clarity.

to alkoxide formation by analogous Brønsted acid–base reactions (Extended Data Fig. 7 and vide infra), and the formation of surface alkoxide species is further corroborated by solid-state 1D and 2D ^{1}H and ^{1}H{^{13}C} magic angle spinning (MAS) NMR (Fig. 3c, Extended Data Fig. 7b,c and Methods).

We next turned to transmissive Fourier transform infrared (FTIR) spectroscopy to quantify the extents to which different olefins interact with the catalyst's Brønsted acid sites. The proposed silanol–olefin Brønsted acid–base reaction to yield surface alkoxides should consume surface silanol groups in a 1:1 stoichiometry, leading to a negative absorbance peak in the Si–OH region that can be quantified using a known integrated molar extinction coefficient ($\varepsilon = 1.4 \pm 0.2$ cm μmol^{-1})[24]. Exposure of fresh 3%SOMC to 10% propylene and He at 50 °C, followed by purging under flowing He, led to a 4 ± 1 μmol per gram of catalyst (g_{cat}) Si–OH consumption (Fig. 3b, blue), or equivalently a 4 ± 1 μmol per g_{cat} surface coverage of isopropoxy groups. Repeating this experiment with different olefins led to Si–OH consumptions of 0.5 ± 0.1 μmol per g_{cat} (10% ethylene), 31 ± 5 μmol per g_{cat} (10% isobutene) and 33 ± 5 μmol per g_{cat} (0.85% 4ME + 0.15% i4ME) (Fig. 3b). This trend (ethylene < propylene < isobutene ≅ 4MEs) can be rationalized in terms of increasing ease to generate the carbocation on olefin protonation and subsequently the surface alkoxide species, while also matching that of promotional ability (Fig. 1, bottom). This highlights the importance of Brønsted acidic silanols in modulating the dynamic balance between site renewal and decay. Indeed, early experiments demonstrated that steady-state propylene metathesis rates can be increased by poisoning these acidic sites, whether reversibly by co-feeding ammonia[25] or irreversibly by introducing a silylating agent[26]. Similarly, besides the promoter's Brønsted basicity, the underlying catalyst's Brønsted acidity may also affect the steady-state metathesis activity.

A putative mechanism for Brønsted acid-catalysed site renewal and decay is the 1,2-proton shift pathway (Extended Data Fig. 8a) that has been extensively documented for tantalum, molybdenum and tungsten complexes in the presence of a proton source[27–29] and proposed for the low-temperature initiation of styrene metathesis on well-defined silica-supported W(IV)-oxo species[22]. This process has been shown to be readily reversible[22,29], consistent with the site initiation and decay pathways proposed here. Preliminary computations also concur that proton transfer from an adjacent silanol group could initiate restoration of the catalytically active sites (Extended Data Fig. 8).

A catalytic mechanism integrating the Chauvin cycle with dynamic site renewal and decay, while illustrating a possible role of the promoter olefin, is presented in Fig. 4. In the absence of promoter, site renewal and decay (blue) are mediated by proximal silanol groups (red) by means of the hydride shift mechanism described above, resulting in a dynamic balance that governs the fraction of Chauvin cycle intermediates (black) and hence the observed metathesis rate. Disubstituted alkylidenes, such as the isopropylidene pictured, are competent metathesis initiators[30] and can lead to the main Chauvin cycle after a single turnover (bottom left). Free silanol groups react with promoter olefins to yield the alkoxide and/or carbocation species (green) observed by DRIFTS and solid-state NMR. As acid–base pairs, these species serve as kinetically superior proton transfer agents compared to free surface silanols, akin to the role of $[PhNMe_2H][B(C_6F_5)_4]$ as an initiator of molecular metathesis catalysts[29]. Although the precise mechanism by which these acid–base pairs facilitate proton transfers remains under investigation, this mechanism is nevertheless fully consistent with all of our experimental observations (Methods).

The practicality of our mechanism is demonstrated by the reactivity gains obtained using impregnated catalysts both for the self-metathesis of propylene and for the industrially relevant cross-metathesis of ethylene and 2-butene (Extended Data Figs. 2c–e and 9). Co-feeding the 4ME promoter over a 3 wt% WO_3/SiO_2 catalyst (prepared by incipient wetness impregnation) at 250 °C resulted in a rate increase of roughly nine times, and comparable results were obtained over a 15 wt% industrial catalyst. These values are lower than those obtained with 3%SOMC (roughly 30×), even though both synthetic protocols yield isolated metal sites at low loadings. The differences are attributed to the absence of water-driven dissolution and/or precipitation and surface restructuring phenomena during the SOMC synthesis, which can alter the local environment and corresponding reactivity of isolated metal sites. Nevertheless, the results clearly show the use of promoters as a versatile handle to access reaction conditions previously considered impractical for tungsten-based materials.

Finally, similar reactivity gains are also observed for molybdenum-based materials, confirming that our observations and proposed mechanism are indeed universal. Steady-state propylene metathesis rates increased by roughly 26× and 68× on co-feeding the 4MEs promoter at 200 °C over a 1.5 wt% MoO_3/SiO_2 catalyst prepared by SOMC (1.5% MoSOMC) and a 1.4 wt% MoO_3/SiO_2 catalyst prepared by incipient wetness impregnation, respectively (Extended Data Fig. 10).

Online content

Any methods, additional references, Nature Portfolio reporting summaries, source data, extended data, supplementary information, acknowledgements, peer review information; details of author contributions and competing interests; and statements of data and code availability are available at https://doi.org/10.1038/s41586-023-05897-w.

1. Copéret, C. et al. Olefin metathesis: what have we learned about homogeneous and heterogeneous catalysts from surface organometallic chemistry? *Chem. Sci.* **12**, 3092–3115 (2021).
2. Sattler, J. J., Ruiz-Martinez, J., Santillan-Jimenez, E. & Weckhuysen, B. M. Catalytic dehydrogenation of light alkanes on metals and metal oxides. *Chem. Rev.* **114**, 10613–10653 (2014).
3. Agarwal, A., Sengupta, D. & El-Halwagi, M. Sustainable process design approach for on-purpose propylene production and intensification. *ACS Sustainable Chem. Eng.* **6**, 2407–2421 (2018).
4. Carr, C. *Global Propylene Market* http://cdn.ihs.com/www/pdf/asia-chem-conf/Carr.pdf (2014).
5. Tian, P., Wei, Y., Ye, M. & Liu, Z. Methanol to olefins (MTO): from fundamentals to commercialization. *ACS Catal.* **5**, 1922–1938 (2015).
6. Jean-Louis Hérisson, P. & Chauvin, Y. Catalyse de transformation des oléfines par les complexes du tungstène. II. Télomérisation des oléfines cycliques en présence d'oléfines acycliques. *Makromol. Chem. Macromol. Chem. Phys.* **141**, 161–176 (1971).
7. Hoveyda, A. H. & Zhugralin, A. R. The remarkable metal-catalysed olefin metathesis reaction. *Nature* **450**, 243 (2007).
8. Amakawa, K. et al. In situ generation of active sites in olefin metathesis. *J. Am. Chem. Soc.* **134**, 11462–11473 (2012).
9. Lwin, S. & Wachs, I. E. Olefin metathesis by supported metal oxide catalysts. *ACS Catal.* **4**, 2505–2520 (2014).
10. Howell, J. G., Li, Y.-P. & Bell, A. T. Propene metathesis over supported tungsten oxide catalysts: a study of active site formation. *ACS Catal.* **6**, 7728–7738 (2016).
11. Handzlik, J., Kurleto, K. & Gierada, M. Computational insights into active site formation during alkene metathesis over a MoO_x/SiO_2 catalyst: the role of surface silanols. *ACS Catal.* https://doi.org/10.1021/acscatal.1c03912 (2021).
12. Mougel, V. et al. Low temperature activation of supported metathesis catalysts by organosilicon reducing agents. *ACS Cent. Sci.* **2**, 569–576 (2016).
13. Ding, K. et al. Highly efficient activation, regeneration, and active site identification of oxide-based olefin metathesis catalysts. *ACS Catal.* **6**, 5740–5746 (2016).
14. Michorczyk, P., Węgrzyniak, A., Węgrzynowicz, A. & Handzlik, J. Simple and efficient way of molybdenum oxide-based catalyst activation for olefins metathesis by methane pretreatment. *ACS Catal.* **9**, 11461–11467 (2019).
15. Lwin, S. & Wachs, I. E. Catalyst activation and kinetics for propylene metathesis by supported WO_x/SiO_2 catalysts. *ACS Catal.* **7**, 573–580 (2016).
16. Zhao, P. et al. Entrapped single tungstate site in zeolite for cooperative catalysis of olefin metathesis with Brønsted acid site. *J. Am. Chem. Soc.* **140**, 6661–6667 (2018).
17. Copéret, C. Single-sites and nanoparticles at tailored interfaces prepared via surface organometallic chemistry from thermolytic molecular precursors. *Acc. Chem. Res.* **52**, 1697–1708 (2019).
18. Poater, A., Solans-Monfort, X., Clot, E., Coperet, C. & Eisenstein, O. Understanding d^0-olefin metathesis catalysts: which metal, which ligands? *J. Am. Chem. Soc.* **129**, 8207–8216 (2007).
19. Luckner, R. C. & Wills, G. B. Transient kinetics of the disproportionation of propylene over a tungsten oxide on silica catalyst. *J. Catal.* **28**, 83–91 (1973).
20. Pennella, F. & Banks, R. L. The influence of chelating polyolefins on the disproportionation of propylene catalyzed by WO_3 on silica. *J. Catal.* **31**, 304–308 (1973).
21. Chatterjee, A. K., Choi, T.-L., Sanders, D. P. & Grubbs, R. H. A general model for selectivity in olefin cross metathesis. *J. Am. Chem. Soc.* **125**, 11360–11370 (2003).
22. Chan, K. W., Mance, D., Safonova, O. V. & Copéret, C. Well-defined silica-supported tungsten (IV)–oxo complex: olefin metathesis activity, initiation, and role of Brønsted acid sites. *J. Am. Chem. Soc.* **141**, 18286–18292 (2019).
23. Amakawa, K., Wang, Y., Kröhnert, J., Schlögl, R. & Trunschke, A. Acid sites on silica-supported molybdenum oxides probed by ammonia adsorption: experiment and theory. *Mol. Catal.* **478**, 110580 (2019).
24. Gabrienko, A. A. et al. Direct measurement of zeolite Brønsted acidity by FTIR spectroscopy: solid-state 1H MAS NMR approach for reliable determination of the integrated molar absorption coefficients. *J. Phys. Chem. C* **122**, 25386–25395 (2018).
25. Gangwal, S. K. & Wills, G. B. Effects of ammonia and amines on propylene disproportionation over a tungsten oxide silica catalyst. *J. Catal.* **52**, 539–541 (1978).
26. Van Roosmalen, A. & Mol, J. Active centers for the metathesis and isomerization of alkenes on tungsten-oxide/silica catalysts. *J. Catal.* **78**, 17–23 (1982).
27. Freundlich, J. S., Schrock, R. R., Cummins, C. C. & Davis, W. M. Organometallic complexes of tantalum that contain the triamidoamine ligand, $[(Me_3SiNCH_2CH_2)3N]3$-, including an ethylidene complex formed via a phosphine-catalyzed rearrangement of an ethylene complex. *J. Am. Chem. Soc.* **116**, 6476–6477 (1994).
28. Hirsekorn, K. F. et al. Thermodynamics, kinetics, and mechanism of (silox) 3M (olefin) to (silox) 3M (alkylidene) rearrangements (silox=tBu3SiO; M=Nb, Ta). *J. Am. Chem. Soc.* **127**, 4809–4830 (2005).
29. Liu, S., Boudjelel, M., Schrock, R. R., Conley, M. P. & Tsay, C. Interconversion of molybdenum or tungsten d2 styrene complexes with d0 1-phenethylidene analogues. *J. Am. Chem. Soc.* **143**, 17209–17218 (2021).
30. Taylor, J. W., Schrock, R. R. & Tsay, C. Molybdenum disubstituted alkylidene complexes. *Organometallics* **39**, 658–661 (2020).

Methods

Catalyst synthesis

The synthesis and characterization of the W-oxo (3%SOMC) and Mo-oxo (1.5%MoSOMC) SOMC–TMP catalysts used in this study have been previously reported[12,31]. The synthesis of these materials by the SOMC–TMP approach leverages a selective reaction between tungsten (or molybdenum) siloxide precursor complexes and the isolated surface silanol groups of partially dehydroxylated silica. This protonolysis reaction is accompanied by the evolution of 1 equivalent of the corresponding alcohol that can be measured by NMR analysis of the supernatant, although often only roughly 0.7–0.8 equivalents are observed due to in situ decomposition catalysed by the acidic metal centres. Depending on the choice of precursor and extent of dehydroxylation of the support, grafting can sometimes also take place by means of the ring-opening of strained siloxane (Si–O–Si) bridges that yields new Si–OR and/or Si–R moieties[32]; however, such chemistry was not observed as main grafting pathways for our materials. Subsequently, thermal treatment of the grafted precatalyst under high vacuum yields the desired isolated silica-supported W(VI)-oxo and W(VI)-dioxo sites in a 1:1 ratio, as determined by X-ray absorption spectroscopy in previous work[12]. It is this thermal decomposition step that distinguishes the SOMC–TMP approach from the conventional SOMC approach in which the grafted materials are the actual catalysts. Furthermore, the decomposition of residual siloxide ligands into silica during the thermal treatment can also alter the silica surface chemistry and possibly contribute to the presence of proximal silanol groups.

The incipient wetness impregnation (IWI) MoO_x/SiO_2 catalyst was prepared as follows. The silica gel support (Sigma-Aldrich, Davisil Grade 646, pore size 150 Å, 300 $m^2\,g^{-1}$) was calcined in air (60 ml min^{-1}, Airgas, dry air) at 500 °C (3 °C min^{-1}) for 3 h and sieved. Particles sized from 40–60 mesh were kept for further catalyst synthesis. A solution of 0.0753 g of ammonium molybdate tetrahydrate (Fluka, ≥99%) in water (4 ml, milli-Q, purified by Thermo Scientific, Barnstead Nanopure system) was added dropwise to 2.0757 g of SiO_2 (calcined, 40–60 mesh) support. The slurry was slowly stirred at room temperature until no obvious colour gradient was observed and then dried at room temperature for 6 h. Next, the slurry was dried at 90 °C (1 °C min^{-1}) for 3 h and calcined at 400 °C (1 °C min^{-1}) in air (60 ml min^{-1}, Airgas, dry air, additional purification by moisture trap, Restek 22014) for 3 h. After the calcination, the catalyst was sieved again to keep the particle size range from 40 to 60 mesh. The Mo loading (1.4 wt% Mo) of the catalyst was confirmed by inductively coupled plasma–optical emission spectrometry.

The 3% WO_x/SiO_2 IWI catalyst was prepared in the same manner as the IWI Mo catalysts. The same silica support (Aerosil 200) as WSOMC was used. The silica support was washed with milli-Q water and calcined to 550 °C (5 °C min^{-1}) for 3 h. To achieve 3 wt% W loading, a solution of 0.0884 g of ammonium metatungstate hydrate (Sigma-Aldrich, 99.99% trace metals) was added dropwise to 2.0132 g of SiO_2. After stirring, the slurry was dried at 90 °C (1 °C min^{-1}) for 3 h and calcined at 400 °C (1 °C min^{-1}) under flowing air (60 ml min^{-1}) for 3 h. After the calcination, the 3%WIWI catalyst was sieved to ensure particle size ranged between 40 and 60 mesh. As discussed in the main text, although both the SOMC–TMP and IWI syntheses lead to isolated metal-oxo sites at low metal loadings, the observed reactivity differences point to subtle variations in molecular structure that are not yet fully understood.

Edge energy analysis using in situ UV–vis spectroscopy

The in situ ultraviolet-visible light (UV–vis) spectrum was acquired on a Cary 5000 UV–vis–near-infrared spectrophotometer. The UV–vis spectrum was collected relative to a baseline of $BaSO_4$ measured under ambient conditions. 3%SOMC was loaded into the sample holder and placed into the DiffusIR environmental chamber (PIKE Technologies, 162–4200), which was sealed by two-way bellows sealed valves (Swagelok, SS-4H), inside the glovebox. Before experiments, the catalyst was heated to 450 °C (1 °C min^{-1}) for 2 h and cooled to 30 °C under flowing 50 ml min^{-1} purified air.

The reflectance spectra from UV–vis spectroscopy were converted to Kubelka–Munk function using the following equation. The edge energy for direct allowed transitions was the y-intercept of a straight line fitted at the low-energy rise of a plot of $[F(R_\infty)h\upsilon]^2$ as a function of $h\upsilon$ (photon energy)[33].

$$F(R_\infty) = \frac{(1-R_\infty)^2}{2R_\infty}$$

Raman spectroscopy

To confirm the absence of WO_3 crystallites that could potentially contribute to surface Brønsted acidity, in situ Raman spectra were acquired using a Renishaw Invia Reflex Micro Raman equipped with a 532 nm laser. 3%SOMC was loaded in a Raman High-Temperature Reaction chamber (Harrick Scientific, HVC-MRA-5), which was sealed using two-way bellows sealed valves (Swagelok, SS-4H), inside the glovebox. Spectra were obtained at a resolution of 2 cm^{-1} at room temperature using a laser power of 5 mW with an accumulation of 20 scans. Dehydration of the catalyst was performed by heating the catalyst to 450 °C (1 °C min^{-1}) for 2 h and cooled to room temperature under flowing 50 ml min^{-1} purified air. Owing to strong fluorescence from the SiO_2 support, the exact molecular structure of isolated surface WO_x sites cannot be inferred from Raman spectra alone, but our previous X-ray absorption spectroscopy study[12] confirms that 3%SOMC consists of a 1:1 mixture of W(VI)-oxo and W(VI)-dioxo sites.

The Raman spectra under ambient conditions were recorded with the same instrument set-up. Instead of an in situ cell, the samples were sandwiched between two glass sample holders.

Reactor set-up

Loading of moisture-sensitive SOMC catalysts was performed inside an N_2-filled glovebox to minimize atmospheric contact. (The wet-impregnation catalysts were loaded outside the glovebox under standard atmospheric conditions.) In a typical procedure, 10 mg of tungsten catalyst was mixed with 40 mg of $SiO_{2\text{–}700}$ (inert catalyst support) to ensure a uniform bed. For the molybdenum catalysts, 20 mg of catalyst was mixed with 100 mg of SiC (46 grit, Alfa Aesar, used as received). The catalyst particle size was controlled by presieving the silica support to 40–60 mesh (vide supra; the particle size remains largely unchanged over the course of the synthesis, and the strong static environment in the glovebox precluded postsynthesis sieving). The industrial catalyst was pelletized and sieved to 40–60 mesh and used in large enough amounts that dilution was not necessary. The mixture was packed between two sets of 200 mg inert SiC (46 grit, Alfa Aesar, used as received) and two 50 mg quartz wool plugs (Technical Glass Products, 4–6 μm) into a U-shaped stainless steel tube (SS304, 0.25 inches outer diameter, 0.18 inches inner diameter). A K-type thermocouple (Omega Engineering) was then fitted above the bed and its height adjusted such that its tip just touches the top end of the bed. Both ends of the U-tube were then fitted with shut-off valves and the packed reactor transferred out of the glovebox. The packed reactor was then connected to the inlet and outlet manifolds such that the gas flows downwards through the bed, which remains stationary in a fixed-bed configuration.

Reactor inlet flows

Flows of propylene (Airgas, CP grade), helium (Airgas, UHP 5.0 grade), 2-butene (Airgas, CP grade, a mixture of *cis*- and *trans*-isomers), ethylene (Airgas, CP grade), isobutene (Airgas, CP grade) and synthetic air

(Airgas, dry) were controlled by a set of mass flow controllers (Brooks SLA5800 with 0254 controller) calibrated to each individual gas. Promoters in the liquid state at room temperature and pressure, namely 4ME (Sigma-Aldrich, more than 99%) and i4ME (TCI Chemicals, more than 98%), were introduced by bubbling helium through a 100 ml stainless steel bubbler filled with the liquid promoter and immersed in a temperature-controlled cooling bath. By saturating the helium flow with the vapour pressure of the promoter, this procedure allows for more consistent promoter concentrations than can be achieved by a syringe pump. All inlet gas flows except air were purified by passing through individual traps containing 3 Å molecular sieves and pre-activated BASF R3-11G catalyst to remove water and oxygen, respectively. Dry air was further purified by passing through a moisture trap (Restek, 22014) to remove water. Liquid promoters were stored over 3 Å molecular sieves inside the glovebox and briefly treated (roughly 5 min) with BASF Selexsorb CD to remove traces of oxygenates before loading into the bubbler (extended contact catalysers isomerization and should be avoided).

Reaction procedure

The reactor set-up was carefully checked for leaks before starting each run. In a typical procedure for tungsten-based catalysts, the catalyst was first pretreated under 100 ml min^{-1} helium for 1 h at the pretreatment temperature using a ramp rate of 5 °C min^{-1}. Heating was provided by a temperature-controlled tube furnace (Carbolite GTF 11/50/150; Digi-Sense 89000) fitted with a custom-made aluminium block, which we have found to be essential for obtaining reproducible results, to fill remaining void space and improve heat transfer. After pretreatment, the furnace was cooled down to the reaction temperature over 2 h, and the gas flow was switched to the desired reacting gas mixture on reaching reaction temperature. For safety reasons, pretreatment was performed without the block in runs where the pretreatment temperature exceeded 500 °C, with the block only inserted after the prescribed pretreatment duration. For the molybdenum-based catalysts, the catalyst bed was first calcined under 40 ml min^{-1} air for 3 h at 400 °C with a temperature ramp rate of 1 °C min^{-1}. After calcination, the reactor was cooled down to 270 °C in air and purged with 100 ml min^{-1} helium for 1 h. Then, the catalyst was pretreated under the same helium flow for 3 h at 500 °C with a ramp rate of 2 °C min^{-1}. After pretreatment, the catalyst was cooled to reaction temperature and the gas flow was switched to reaction conditions. Here, a home-built furnace was equipped with the controller (Digi-Sense 89000) to provide heating. To build the furnace, a stainless steel tube (SS316, 2.5 inches outer diameter, 6.0 inches long) was wrapped with a heating tape (Omega, High Temperature, Dual-Element), and subsequently insulated by wrapping 1-inch thick ceramic fibre insulation sheets. The application of different furnaces here induced negligible difference (less than 5%) in measured catalyst activities.

Kinetic studies

The effluent gases were analysed by gas chromatography (GC) (Shimadzu GC-2014 equipped with an Agilent HP-PLOT Al_2O_3-S (30 m × 0.25 mm) column) with injections at roughly 15-min intervals. Products were identified by comparing retention times to known standards and quantified by means of a flame ionization detector (FID) calibrated against known standards. The propylene concentration was varied by adjusting the flow rates of propylene and helium at a constant total flow rate and inferred from Dalton's law. The equations used to calculate the reaction rate are presented below. For promoted runs, the promoter concentration was adjusted by varying the fraction of helium flow through the bubbler while keeping the total helium flow rate and propylene flow rate constant. The promoter concentration was inferred from its FID peak area when bypassing the reactor (note below in the next paragraph). The mass balance of all data points closes within the expected uncertainties of the flow rates, and the introduction of promoter does not significantly affect the mass balance, confirming that only a small fraction of promoter is converted into other products (see Extended Data Table 1a for a detailed analysis of a typical run).

Note that the GC column used for product analysis is optimized for light hydrocarbon separations and does not separate 4ME and i4ME even after extensive method tuning. Hence, to determine relative concentrations of 4ME and i4ME, the effluent was bubbled through a stainless steel bubbler containing acetone, which was then analysed by a second GC–FID (Agilent 7890A with a DB-1701 column better able to separate larger organic molecules). Peak assignment and response factors were determined from pure standards, and the relative 4ME and i4ME concentrations in each sample inferred from peak area ratios. This procedure relies on complete miscibility between 4ME, i4ME and acetone and identical vapour-liquid mass transfer rates, which is probably a very good assumption considering the chemical similarity of i4ME and 4ME.

A blank experiment with the inert SiC packing and SiO_2 support but without catalyst showed no propylene conversion at 350 °C. Irreversible deactivation was not observed over the time scale of our experiments and accordingly not considered in our fitting of kinetic parameters. This also precludes the possibility of sintering and/or coking as possible contributors to active site decay in our system. Although a small amount of coke may be formed, as evidenced by a noticeable blackening of the spent catalyst, such carbonaceous deposits typically do not have a noticeable effect on the metathesis activity of WO_x/SiO_2 (ref. 34).

The weight hourly space velocity (WHSV, in mol C_3H_6 per g_{cat} s^{-1}) is defined as:

$$\mathrm{WHSV} = \frac{Q_{C_3H_6}}{22.4 m_{cat}}$$

where $Q_{C_3H_6}$ is the volumetric flow rate of propylene (l s^{-1}), m_{cat} is the mass of catalyst loaded (g) and 22.4 l mol^{-1} is the molar volume of an ideal gas at standard temperature and pressure.

The reaction rate (mol per g_{cat} s^{-1}) is taken to be the rate of product formation and calculated as follows:

$$\mathrm{rate} = \frac{1}{22.4}\frac{Q_{total} y_{products}}{m_{cat}}$$

where Q_{total} is the total volumetric flow rate (l s^{-1}), $y_{products}$ is the sum of ethylene, *cis*-butene and *trans*-butene mole fractions as determined by GC–FID peak areas and calibrated response factors, 22.4 l mol^{-1} is the molar volume of an ideal gas at standard temperature and pressure and m_{cat} is the mass of catalyst loaded (g).

The inability to control the particle size during catalyst loading, or to control the tungsten loading without affecting the active site speciation, prevent the application of direct tests, such as the Madon–Boudart test, for transport limitations. Nevertheless, the observation of high-order kinetics, high activation energies and the promotional effect all strongly indicate operation in a kinetically limited regime. Furthermore, temperature gradients are unlikely to be significant because the metathesis reaction is nearly isothermal. To support these claims, we have tabulated representative physical parameter values in Extended Data Table 2 and applied theoretical criteria for assessing potential transport limitations as follows:

Weisz–Prater criterion[35] (second-order reaction) for excluding internal mass transfer limitations (all parameters are as defined in Extended Data Table 2):

$$\frac{r_p^2 r'''}{D_e C_A} = \frac{(2\times10^{-4})^2 (80)}{(4\times10^{-6})(10)} = 0.08 < 0.3$$

Mears criterion[36] for excluding external mass transfer limitations (all parameters are as defined in Extended Data Table 2):

$$\frac{r_p r'''}{k_m C_A} = \frac{(2\times10^{-4})\,(80)}{(0.1)\,(10)} = 0.016 < 0.15$$

Mears criterion[36] for excluding heat transfer limitations (all parameters are as defined in Extended Data Table 2):

$$\frac{|\Delta H_r| r_p\, r'''}{hT}\frac{E_a}{RT} = \frac{(6{,}000)(2\times10^{-4})(80)}{(1{,}000)(603)}\frac{2\times10^5}{(8.314)(603)} = 0.008 < 0.15$$

DRIFTS

DRIFTS spectra were acquired using a Bruker Vertex 70 FTIR spectrometer equipped with a Praying Mantis High-Temperature Reaction Chamber (HVC-DRM-5, Harrick Scientific). Samples were loaded inside a diffuse reflectance cell (Harrick, HVC) inside a glovebox. As with the U-tube reactor set-up, inlet and outlet valves enable complete isolation from the atmosphere over the entire process. To obtain spent catalyst, standard reaction conditions in the U-tube reactor were replicated as closely as possible in the DRIFTS cell. Fresh 3%SOMC was treated under 50 ml min^{-1} N_2 at 500 °C (5 °C min^{-1}) for 1 h, cooled to 350 °C, exposed to 50 ml min^{-1} C_3H_6 for 12 h, purged with 50 ml min^{-1} N_2 for 1 h to remove chemisorbed species, then finally cooled to 50 °C to yield spent catalyst. In a typical experiment, the spent catalyst was contacted with 50 ml min^{-1} of the specified olefin gas blend for 3 h, then purged with 50 ml min^{-1} N_2 to remove gas-phase and physisorbed olefins until no further spectral changes were observed (typically several hours). Deviations to this procedure in control experiments are described in the captions of the relevant figures.

In situ FTIR

In situ FTIR spectra were acquired on a Bruker Vertex 70 spectrometer equipped with a liquid N_2 cooled Hg-Cd-Te (MCT) detector. All infrared spectra were collected relative to an empty cell spectrum measured at 50 °C under flowing helium. The 3%SOMC catalyst powder (7–10 mg) was pressed into 7 mm diameter wafers and loaded into a high-temperature transmission infrared cell (Harrick Scientific Products Inc.) sealed with KBr windows (32 × 3 mm; Harrick Scientific Products Inc.) and two-way bellows sealed valves (Swagelok, SS-4H) inside the glovebox. Before the experiment, the catalyst was heated to 450 °C (1 °C min^{-1}) for 2 h and cooled to 300 °C under flowing 50 ml min^{-1} air. Then, the catalyst was purged at 300 °C under flowing 50 ml min^{-1} helium, cooled to 50 °C, and exposed to 50 ml min^{-1} of the specified gas mixture until the steady-state spectrum was obtained. The catalyst was purged under flowing 50 ml min^{-1} helium again until the steady-state spectrum was obtained and heated to 80, 120, 160 and 200 °C (5 °C min^{-1}) stepwise. A steady-state spectrum was collected at each temperature.

The Si–OH consumption was estimated using the following equation with an integrated molar extinction coefficient (ε) of 1.4 ± 0.2 cm μmol^{-1} (ref. 24).

$$\text{Si}-\text{OH}\ (\mu\text{mol per g}_{cat}) = \frac{A}{\varepsilon}\times\frac{W}{m}$$

In the equation above, A (cm^{-1}) is the area of the negative peak of Si–OH; W (cm^2) is the cross area of the catalyst pellet and m (g) is the mass of the catalyst pellet. Band broadening and catalyst darkening on olefin adsorption may lead to slight deviations from this idealized Beer–Lambert relationship but do not affect the conclusions derived in our study, namely that the trend in chemisorption ability among different olefins matches that of the promotional ability.

^{15}N-pyridine adsorption and solid-state ^{15}N{^{1}H} extended CPMAS NMR

^{15}N-pyridine (99% isotopic enrichment) was purchased from CortecNet Corp., dried over CaH_2 at 60 °C overnight and degassed before use. For the adsorption of ^{15}N-pyridine, roughly 50 mg of catalyst was loaded into a small glass vessel with a magnetic stir bar and placed under high vacuum (less than 10^{-4} mbar). The vessel was sealed and exposed to vapour pressure of ^{15}N-labelled pyridine at room temperature for 15 min while stirring. The catalyst was then evacuated under high vacuum for at least 1 h, after which it was transferred into an argon-filled glovebox and packed into a sapphire LTMAS NMR rotor with a zirconia drive cap. The rotor was transferred to the NMR spectrometer in a tightly sealed vial with a screw-cap top, rapidly inserted into the precooled MAS NMR probehead and spun with dry N_2 gas at 100 K. The 1D ^{15}N{^{1}H} CPMAS NMR spectra were acquired on a 600 MHz (14.1 T) Bruker DNP NMR spectrometer equipped with a 3.2 mm HXY low-temperature MAS NMR probehead and operating at Larmor frequencies of 60.803 and 599.900 MHz for ^{15}N and ^{1}H, respectively. The ^{15}N{^{1}H} CPMAS spectra were acquired with ^{15}N{^{1}H} contact times of 3 ms, at 10 kHz MAS and with 100 kHz SPINAL-64 ^{1}H heteronuclear decoupling during the acquisition periods. Relaxation delays were set to roughly 1.4 times the longest measured ^{1}H spin-lattice T_1 relaxation time measured by ^{1}H saturation recovery.

Solid-state ^{1}H/^{1}H{^{13}C} CPMAS NMR

Here, 2,3-dimethyl-1-butene (i4ME; TCI Chemicals, less than 98%) was dried over CaH_2 at 60 °C overnight, briefly treated with BASF Selexsorb CD, and degassed immediately before use. The catalyst (roughly 50 mg) was loaded into a small quartz vessel and reduced thermally under high vacuum (700 °C, 5 °C min^{-1}, 1 h, less than 10^{-4} mbar). The reduction was accompanied by a slight colour change from white to light blue. The reduced catalyst was then cooled to room temperature and evacuated under high vacuum. i4ME was introduced by quickly flashing the liquid into the evacuated vessel until a pressure of 100 mbar was reached. Subsequently, propylene was added to a total pressure of 500 mbar. As a safety note, subatmospheric pressures were used in view of possible overpressure on heating the sealed vessel. In the control experiment, only propylene was added to a pressure of 500 mbar. The vessel containing the reduced catalyst and the olefin mixture was then isolated, briefly heated by immersing for 5 min in a tube furnace preheated to 250 °C, cooled to room temperature and finally evacuated under high vacuum for 1 h. The samples were transferred into an Ar-filled glovebox and analysed within 24 h of preparation to minimize potential decay of surface species.

The 1D and 2D solid-state ^{1}H and ^{1}H{^{13}C} NMR spectra were acquired on a 400 MHz (9.4 T) Bruker NMR spectrometer equipped with a 1.3 mm HXY MAS probehead and operating at Larmor frequencies of 100.648 and 400.231 MHz for ^{13}C and ^{1}H, respectively. The 2D NMR spectra resolve correlated signals from proximate (less than 0.5 nm) ^{13}C–^{1}H spin pairs on the catalyst surface that are dipole–dipole coupled, being primarily sensitive to interactions of covalently bonded species. Signal sensitivity is enhanced by fast-MAS and indirect detection techniques[37,38], which enable acquisition of the 2D spectra despite low natural abundance of ^{13}C (1.1%) and low quantities of surface carbon. The as-prepared samples (vide supra) were ground using a ceramic mortar and packed into 1.3 mm NMR rotors. The rotor was transferred to the NMR spectrometer in a tightly sealed vial with a screw-cap top, rapidly inserted into the MAS probehead, and spun with dry N_2 gas at ambient temperature. The 1D ^{1}H MAS NMR spectra was monitored over the course of the measurement period to confirm minimal degradation of the sample. MAS rates of 40 kHz were used with relaxation delays of 0.75 s, which was roughly 1.4 times the longest measured ^{1}H spin-lattice T_1 relaxation time (measured by ^{1}H saturation recovery). The measurements used ^{1}H π/2 pulse lengths of 1.4 μs (180 kHz) and ^{13}C π/2

pulse lengths of 3 μs (83 kHz). The 2D $^{1}H\{^{13}C\}$ correlation spectrum was acquired using a 2D dipolar-mediated heteronuclear multiple quantum coherence (D-HMQC) sequence with 60 rotor periods of SR4 recoupling[39] to reintroduce the $^{1}H-^{13}C$ dipole–dipole couplings. Arbitrary indirect detection was applied in the indirect dimension to mitigate sensitivity loss due to T_2 relaxation[40]. Then 32 T_1 increments were used in the indirect dimension and 6,144 transients for a total acquisition time of 41 h. The 1D ^{1}H spin echo MAS NMR spectra were acquired with 1.5 s relaxation delays and rotor-synchronized echo delays of 0.05 ms (two rotor periods).

Assignment of solid-state 2D NMR peaks

3%SOMC was activated thermally and subsequently contacted with i4ME and propylene (see above for sample preparation details). ^{1}H MAS NMR signals are detected at 0.6, 1.0, 1.6 and 5.4 ppm (Fig. 3c), which are resolved on the basis of their different correlations to ^{13}C signals in the solid-state 2D $^{1}H\{^{13}C\}$ D-HMQC NMR correlation spectra of the postreaction catalyst. Specifically, the ^{1}H signals at 0.6, 1.0 and 1.6 ppm are all correlated to a distribution of ^{13}C signal intensity from 20 to 35 ppm (green shaded region in Fig. 3c), which we assign to a distribution of surface alkyl moieties, possibly derived from hydrocarbon products of olefin aromatization and/or cracking. The ^{1}H signal at 1.6 ppm is also correlated to a ^{13}C signal at 75 ppm (blue shaded region in Fig. 3c), which we assign to surface alkoxide species that are probably bound to the silica support as evidenced by the chemical shift value (that is, close to that of the parent alcohol, in contrast to tungsten-bound alkoxides, which will be significantly deshielded)[41] and significant consumption of silanol groups as observed by FTIR and discussed in the main text. An additional correlation is observed between a ^{1}H signal at 5.4 ppm and ^{13}C signals from 20 to 35 ppm that probably arises from residual surface-bound olefinic moieties. The alkoxide signal was not observed in the corresponding control experiment without i4ME (Extended Data Fig. 7b,c), consistent with our FTIR studies suggesting that the promoter greatly increases the surface coverage of alkoxide species.

Simplified steady-state kinetic model

Consider the reaction network shown in Extended Data Fig. 4. Here we derive a simplified steady-state kinetic model that explicitly illustrates how our proposed mechanism is consistent with our experimental observations. We define 'active sites' as Chauvin intermediates (that is, **1**–**4** in Extended Data Fig. 4), and 'total available sites' as Chauvin intermediates plus metathesis-inactive, off-cycle intermediates. For simplicity, all species within the proposed site decay and/or renewal cycle, including various π complexes and metal alkyls, are represented here as a single resting state (**5**). Other off-cycle intermediates that exist in rapid equilibrium with Chauvin intermediates, such as square pyramidal metallacyclobutanes[18], have not been explicitly included in our model as their equilibria are not expected to be influenced by the promoter.

We further assume steady-state operation at differential, kinetically limited conditions and that all available sites are identical, which permits the use of mean-field rate equations. In reality, grafting of isolated metal sites onto amorphous supports will lead to varying degrees of strain and a heterogeneous distribution of site activities that is not easy to accurately model[42–44].

Chauvin kinetics without site renewal and decay. By applying the pseudo-steady-state approximation to the Chauvin cycle assuming the number of active sites remains constant and initially neglecting the site regeneration and decay cycle, the following rate expression for Chauvin metathesis can be derived as per ref. 45.

$$r_m = \frac{\theta_{total} P_{C_3}}{\frac{1}{K_{12}k_{23}} + \frac{1}{K_{34}k_{41}} + \left(\frac{1}{k_{23}} + \frac{1}{k_{41}}\right)P_{C_3}} \quad (1)$$

where r_m is the steady-state metathesis rate, $\theta_{total} = \theta_1 + \theta_2 + \theta_3 + \theta_4$ is the total number of active sites, and P_{C_3} is the partial pressure of propylene (C_3). Following ref. 45, we have also assumed the cycloaddition steps to be in rapid equilibrium with equilibrium constants K_{12} and K_{34}. As discussed in the main text, equation (1) predicts a C_3 reaction order of between 0 and 1, and cannot explain why reaction orders of up to 1.8 have been reported in the literature[10,16,19].

Chauvin kinetics with unpromoted site renewal and decay. We now turn our attention towards our proposed site decay and renewal cycle, considering first the unpromoted version of the cycle (orange cycle in Extended Data Fig. 4). Here, we assume that the site decay and renewal processes can be represented by single elementary steps with arbitrary rate constants:

$$r_d = k_d \theta_3 P_{C_3}^{d} \quad (2)$$

$$r_f = k_f \theta_5 P_{C_3}^{f} \quad (3)$$

where d and f are the reaction orders for site decay and renewal, respectively. This assumption is motivated by the desire to keep the rate expressions relatively simple and the fact that most complicated rate expressions can be adequately fitted by empirical power-laws.

We also assume that the contributions of site renewal and decay by-products (which may include ethylene as depicted in Fig. 4 of the main text) to the overall product formation rate are negligible. This assumption agrees with the consistent observation (within experimental error) of a 1:1 ethylene:2-butene molar ratio across all our unpromoted propylene self-metathesis experiments.

Again applying the pseudo-steady-state approximation to the resting state (**5**) while modifying the site balance accordingly (that is, $\theta_{total} = \theta_1 + \theta_2 + \theta_3 + \theta_4 + \theta_5$ that now represents the total available sites including off-cycle intermediates in addition to the Chauvin intermediates), we obtain

$$r_m = \frac{\theta_{total} P_{C_3}}{\frac{1}{K_{12}k_{23}} + \frac{1}{K_{34}k_{41}} + \left(\frac{1}{k_{23}} + \frac{1}{k_{41}}\right)P_{C_3} + \frac{1}{K_{34}k_{41}}\frac{k_d}{k_f}P_{C_3}^{d-f}} \quad (4)$$

In the overall rate expression above, the first three terms in the denominator can be understood as contributions to the steady-state metathesis rate from the Chauvin cycle, and the fourth term from the site renewal and decay cycle.

To simplify this rate expression, we may make the further assumption that site renewal is rate-limiting, that is, slow relative to both metathesis and site decay. The former assumption ($r_f \ll r_m$) is supported by the results of our transient experiments, specifically Extended Data Fig. 3b, which shows that the renewal of active sites from a freshly purged catalyst surface (that is, one free of active sites where $\theta_{total} = \theta_5$) at 350 °C and 0.5 bar propylene takes place on a time scale of tens of minutes corresponding to the observed induction period. The steady-state metathesis rate under these conditions is 3.2×10^{-5} mol C_3H_6 per g_{cat} s^{-1}, which yields a turnover frequency of 0.20 s^{-1} assuming that all tungsten atoms in the catalyst are available for reaction (which is probably a significant overestimate of the actual number of available sites), and suggests that metathesis turnovers at a given tungsten site take place on a time scale of no longer than several seconds. This back-of-the-envelope calculation validates our assumption that site renewal is slow relative to metathesis.

The latter assumption ($k_f \ll k_d$) has been directly demonstrated in recent experimental studies on molecular Mo- and W-imido olefin and alkylidene complexes by Schrock and coworkers[29], in which (1) least-squares fitting of NMR-derived transient kinetics yielded rate constants for alkylidene protonation that are 1–2 orders of magnitude

higher than those for protonation of the corresponding olefin complexes, and (2) protonation of the alkylidene complexes was, unlike the protonation of the corresponding olefin complexes, observed to be too fast to follow by NMR. These observations can be qualitatively understood in terms of the strong nucleophilic character of early-metal carbene complexes by comparison of the corresponding π complex, where π-back donation only rarely provides a strong nucleophilic character of the carbon bond to the metal[46].

Assuming the above, the red term will dominate the blue terms in equation (4), yielding:

$$r_m = \frac{k_f}{k_d} K_{34} k_{41} \theta_{\text{total}} P_{C_3}^{1+f-d} \quad (5)$$

This simplified overall rate expression provides a rationalization for how the reaction order can exceed 1 for steady-state propylene metathesis. On the basis of our proposed mechanisms for site decay and renewal discussed in the main text, we expect $d \cong 0$ (for example, if decomposition of the alkylidene is unimolecular) and $0 < f < 1$ (for example, if propylene adsorption is kinetically relevant and the surface is sufficiently far away from saturation), which leads to an overall C_3 order of 1–2. The apparent activation energy depends on the activation energies of metathesis, site renewal and site decay steps, and can thus exceed that computed from the Chauvin cycle alone if site renewal has a higher barrier than site decay (as may be expected from the discussion above).

Similarly, we can also show under the same assumptions that the fraction of active sites is also governed by the balance between site renewal and decay and increases with C_3 partial pressure:

$$\frac{\theta_1 + \theta_2 + \theta_3 + \theta_4}{\theta_{\text{total}}} = \frac{k_f}{k_d} P_{C_3}^{f-d} \left(1 + \frac{K_{34} k_{41}}{K_{12} k_{23}} + K_{34} \left(1 + \frac{k_{41}}{k_{23}}\right) P_{C_3}\right) \quad (6)$$

From the equation above, the condition that site renewal is rate-limiting (that is, $k_f/k_d \ll 1$) also leads to the conclusion that most of the available sites exist in their resting state (**5**) as opposed to Chauvin-active states (**1**–**4**). This directly explains why the active site population in heterogeneous metathesis catalysts is typically very low, difficult to accurately titrate (owing to the dynamic interconversion of Chauvin-active and off-cycle states) and susceptible to promotion (by altering k_f/k_d; below).

Chauvin kinetics with promoted site renewal and decay. Now consider the system in the presence of a promoter olefin, for instance 4ME as shown in the blue cycle of Extended Data Fig. 4. The site decay rate expression of equation (2) remains unchanged, whereas an analogous rate expression for 4ME-mediated site renewal can be written as follows:

$$r_{f,4ME} = k_{f,4ME} \theta_5 P_{4ME}^f \quad (7)$$

Repeating the derivation of equation (5) while considering both the promoted and unpromoted pathways for site renewal yields:

$$r_{m,\text{promoted}} = \frac{k_f}{k_d} K_{34} k_{41} \theta_{\text{total}} P_{C_3}^{1+f-d} + \frac{k_{f,4ME}}{k_d} K_{34} k_{41} \theta_{\text{total}} P_{C_3}^{1-d} P_{4ME}^f \quad (8)$$

On the basis of our proposed promoter-assisted proton transfer mechanism for site renewal, we expect the surface coverage of promoter-derived alkoxides to be kinetically relevant. To this end, our FTIR studies clearly show an increased surface coverage of 4ME-derived alkoxides relative to propylene-derived alkoxides. Thus, coupled with our hypothesis that promoter-derived acid–base pairs effect proton transfers more effectively than surface silanol groups alone, we may consider promoted site renewal to be much faster than unpromoted site renewal (that is, $k_{f,4ME} \gg k_f$). This expression then simplifies to:

$$r_{m,\text{promoted}} = \frac{k_{f,4ME}}{k_d} K_{34} k_{41} \theta_{\text{total}} P_{C_3}^{1-d} P_{4ME}^f \quad (9)$$

which indicates that the sum of C_3 and promoter reaction orders should equal the unpromoted C_3 reaction order, consistent with experimental observations.

Equation (9) also ascribes a physical meaning to the observed promotion factor (PF): for a given promoter concentration, the promotion factor is governed solely by how fast it makes active sites relative to propylene:

$$\text{PF} = \frac{r_{m,\text{promoted}}}{r_m} = \frac{k_{f,4ME}}{k_f} \left(\frac{P_{4ME}}{P_{C_3}}\right)^f \quad (10)$$

By direct comparison to equation (6), we see that the active site fraction increases with the promoter concentration:

$$\frac{\theta_1 + \theta_2 + \theta_3 + \theta_4}{\theta_{\text{total}}} = \frac{k_{f,4ME}}{k_d} P_{4ME}^f P_{C_3}^{-d} \left(1 + \frac{K_{34} k_{41}}{K_{12} k_{23}} + K_{34} \left(1 + \frac{k_{41}}{k_{23}}\right) P_{C_3}\right) \quad (11)$$

Finally, by applying the definition of the apparent activation energy ($E_{a,app}$) to this expression, the experimentally observed decrease in $E_{a,app}$ in the presence of promoter can be attributed to a decrease in the apparent site renewal barrier ($E_{a,f}$) associated with the kinetically relevant proton transfer steps of Fig. 4 in the main text:

$$E_{A,app,\text{promoted}} - E_{a,app} = E_{a,f,4ME} - E_{a,f} \quad (12)$$

Computational studies

Active site model. In this work, we adopt a minimal cubic silsesquioxane cluster model with eight-membered rings comprising each 'face' (Extended Data Fig. 8a, bottom left) to probe the effect of a proximal silanol group on alkylidene formation and decay. Whereas this model may suffice for an initial qualitative evaluation of the relative feasibility of various reaction pathways, it should be noted that the accurate computational treatment of amorphous silica supports remains an open question[47].

Computational methods. All calculations were performed with the ORCA v.4.2 (refs. 48,49) package using the PBE0 functional[50,51] and a composite basis set comprising the def2-SVP (ref. 52) (Si, O) and def2-TZVPP (W, C, H) basis sets. The def2-TZVPP basis set for W includes Stuttgart effective core potentials[53] that provide an approximate treatment of scalar relativistic effects. Zero point vibrational energy and thermal contributions, as determined under the default quasi-harmonic approximation[54] (that is, treating all frequencies below 35 cm^{-1} as free rotors instead of harmonic vibrations), were obtained from analytical frequency calculations on the density functional theory geometries at the same level of theory and added to the electronic energies to yield the enthalpies reported in the main text. Entropic contributions (that is, to yield Gibbs free energies) were omitted because computed values for small cluster models are not directly translatable to actual catalyst supports. The RIJCOSX approximation[55], together with the def2/J series of auxiliary basis sets[56] for geometry optimizations and automatically generated auxiliary basis sets[57] for single-point energy calculations, was used to speed up all calculations. All calculations used the Grid7 grid size setting.

Geometry optimizations used the L-BFGS algorithm in redundant internal coordinates to the default tolerances of 3×10^{-4} hartree per bohr for the maximum gradient and 5×10^{-6} hartree for the change in self-consistent field energy between steps, and characterized with

vibrational frequency analysis to confirm no imaginary frequencies. Transition states were obtained with partitioned rational function optimization (P-RFO)[58], again in redundant internal coordinates, and characterized with vibrational frequency analysis to confirm a single imaginary frequency. Cartesian coordinates of all optimized geometries and tabulated absolute energies are provided as source data.

All intermediates and transition states were simulated as closed-shell singlets. Singlet-triplet gaps were computed for all intermediates and found to be more than 20 kcal mol^{-1}; hence, only the singlet spin surface was studied. Only the lowest-energy conformer of each structure is presented, as the closely spaced (within 1–2 kcal mol^{-1}) conformers with methyl groups in different orientations are expected to freely interconvert under reaction conditions.

Data availability

Source data are provided with this paper. All other data supporting the findings of this study are available from the corresponding authors upon reasonable request.

31. Yamamoto, K. et al. Silica-supported isolated molybdenum di-oxo species: formation and activation with organosilicon agent for olefin metathesis. *Chem. Commun.* **54**, 3989–3992 (2018).
32. Gioffrè, D., Rochlitz, L., Payard, P.-A., Yakimov, A. & Copéret, C. Grafting of group-10 organometallic complexes on silicas: differences and similarities, surprises and rationale. *Helv. Chim. Acta* **105**, e202200073 (2022).
33. Ross-Medgaarden, E. I. & Wachs, I. E. Structural determination of bulk and surface tungsten oxides with UV-vis diffuse reflectance spectroscopy and Raman spectroscopy. *J. Phys. Chem. C* **111**, 15089–15099 (2007).
34. Moodley, D., van Schalkwyk, C., Spamer, A., Botha, J. & Datye, A. Coke formation on WO_3/SiO_2 metathesis catalysts. *Appl. Catal., A* **318**, 155–159 (2007).
35. Weisz, P. & Prater, C. Interpretation of measurements in experimental catalysis. *Adv. Catal* **6**, 60390–60399 (1954).
36. Mears, D. E. Tests for transport limitations in experimental catalytic reactors. *Ind. Eng. Chem. Process Des. Dev.* **10**, 541–547 (1971).
37. Ishii, Y., Yesinowski, J. P. & Tycko, R. Sensitivity enhancement in solid-state 13C NMR of synthetic polymers and biopolymers by 1H NMR detection with high-speed magic angle spinning. *J. Am. Chem. Soc.* **123**, 2921–2922 (2001).
38. Venkatesh, A., Hanrahan, M. P. & Rossini, A. J. Proton detection of MAS solid-state NMR spectra of half-integer quadrupolar nuclei. *Solid State Nucl. Magn. Reson.* **84**, 171–181 (2017).
39. Brinkmann, A. & Kentgens, A. P. Proton-selective 17O–H distance measurements in fast magic-angle-spinning solid-state NMR spectroscopy for the determination of hydrogen bond lengths. *J. Am. Chem. Soc.* **128**, 14758–14759 (2006).
40. Venkatesh, A., Perras, F. A. & Rossini, A. J. Proton-detected solid-state NMR spectroscopy of spin-1/2 nuclei with large chemical shift anisotropy. *J. Magn. Reson.* **327**, 106983 (2021).
41. Noh, G. et al. Lewis acid strength of interfacial metal sites drives CH_3OH selectivity and formation rates on Cu-based CO_2 hydrogenation. *Catalysts. Angew. Chem. Int. Ed.* **60**, 9650–9659 (2021).
42. Goldsmith, B. R., Sanderson, E. D., Bean, D. & Peters, B. Isolated catalyst sites on amorphous supports: a systematic algorithm for understanding heterogeneities in structure and reactivity. *J. Chem. Phys.* **138**, 204105 (2013).
43. Khan, S. A., Vandervelden, C. A., Scott, S. L. & Peters, B. Grafting metal complexes onto amorphous supports: from elementary steps to catalyst site populations via kernel regression. *Reaction Chem. Eng.* **5**, 66–76 (2020).
44. Praveen, C. S., Borosy, A. P., Copéret, C. & Comas-Vives, A. Strain in silica-supported Ga(III) sites: neither too much nor too little for propane dehydrogenation catalytic activity. *Inorg. Chem.* **60**, 6865–6874 (2021).
45. Kapteijn, F., Bredt, H. L., Homburg, E. & Mol, J. C. Kinetics of the metathesis of propene over dirhenium heptaoxide. gamma.-aluminum oxide. *Ind. Eng. Chem. Prod. Res. Dev.* **20**, 457–466 (1981).
46. Gordon, C. P., Andersen, R. A. & Copéret, C. Metal olefin complexes: revisiting the Dewar–Chatt–Duncanson model and deriving reactivity patterns from carbon-13 NMR chemical shift. *Helv. Chim. Acta* **102**, e1900151 (2019).
47. Goldsmith, B. R., Peters, B., Johnson, J. K., Gates, B. C. & Scott, S. L. Beyond ordered materials: understanding catalytic sites on amorphous solids. *ACS Catal.* **7**, 7543–7557 (2017).
48. Neese, F. The ORCA program system. *Wiley Interdiscip. Rev.: Comput. Mol. Sci.* **2**, 73–78 (2012).
49. Neese, F. Software update: the ORCA program system, version 4.0. *Wiley Interdiscip. Rev.: Comput. Mol. Sci.* **8**, e1327 (2018).
50. Perdew, J. P., Burke, K. & Ernzerhof, M. Generalized gradient approximation made simple. *Phys. Rev. Lett.* **77**, 3865 (1996).
51. Adamo, C. & Barone, V. Toward reliable density functional methods without adjustable parameters: the PBE0 model. *J. Chem. Phys.* **110**, 6158–6170 (1999).
52. Weigend, F. & Ahlrichs, R. Balanced basis sets of split valence, triple zeta valence and quadruple zeta valence quality for H to Rn: design and assessment of accuracy. *Phys. Chem. Chem. Phys.* **7**, 3297–3305 (2005).
53. Andrae, D., Haeussermann, U., Dolg, M., Stoll, H. & Preuss, H. Energy-adjusted ab initio pseudopotentials for the second and third row transition elements. *Theor. Chim. Acta* **77**, 123–141 (1990).
54. Grimme, S. Supramolecular binding thermodynamics by dispersion-corrected density functional theory. *Chem. Eur. J.* **18**, 9955–9964 (2012).
55. Neese, F., Wennmohs, F., Hansen, A. & Becker, U. Efficient, approximate and parallel Hartree–Fock and hybrid DFT calculations. A 'chain-of-spheres' algorithm for the Hartree–Fock exchange. *Chem. Phys.* **356**, 98–109 (2009).
56. Weigend, F. Accurate Coulomb-fitting basis sets for H to Rn. *Phys. Chem. Chem. Phys.* **8**, 1057–1065 (2006).
57. Stoychev, G. L., Auer, A. A. & Neese, F. Automatic generation of auxiliary basis sets. *J. Chem. Theory Comput.* **13**, 554–562 (2017).
58. Baker, J. An algorithm for the location of transition states. *J. Comput. Chem.* **7**, 385–395 (1986).
59. Barton, D. G., Shtein, M., Wilson, R. D., Soled, S. L. & Iglesia, E. Structure and electronic properties of solid acids based on tungsten oxide nanostructures. *J. Phys. Chem. B* **103**, 630–640 (1999).
60. McMillan, P. F. & Remmele, R. L. Hydroxyl sites in SiO_2 glass: a note on infrared and Raman spectra. *Am. Mineral.* **71**, 772–778 (1986).
61. Moroz, I. B., Larmier, K., Liao, W.-C. & Copéret, C. Discerning γ-alumina surface sites with nitrogen-15 dynamic nuclear polarization surface enhanced NMR spectroscopy of adsorbed pyridine. *J. Phys. Chem. C* **122**, 10871–10882 (2018).

Acknowledgements The computations were performed on the Euler cluster at ETH Zurich. We acknowledge H. Adamji and J. Zhu for help in the synthesis and characterization of the WI MoO_x/SiO_2 catalyst, T. S. Wesley for a reading of the manuscript and R. R. Schrock for discussions. The work at MIT was financially supported by Saudi Aramco through MIT Energy Initiative (grant no. 6930839). We are grateful to the Swiss National Science Foundation (SNF) for financial support of this work (grant no. 200021L_157146). Z.J.B. also gratefully acknowledges financial support from the SNF (Spark award no. CRSK-2_190322).

Author contributions D.F.C., S.K.S., C.C. and Y.R.-L. conceptualized the project. Y.R.-L. and C.C. supervised the project. Z.J.B. and K.W.C. performed the synthesis and characterization of the SOMC catalysts. Z.J.B. conducted the solid-state NMR analyses. T.Z.H.G., R.Z., J.H.K. and J.R.D.I. performed all other experiments and data analyses. T.Z.H.G. designed and performed the computational studies. T.Z.H.G. wrote the manuscript with input from all other authors.

Competing interests D.F.C., S.K.S. and Y.R.-L. are inventors on a patent application that covers the use of olefin promoters for heterogeneous metathesis. The other authors declare no competing interests.

Additional information

Correspondence and requests for materials should be addressed to Christophe Copéret or Yuriy Román-Leshkov.

Peer review information *Nature* thanks the anonymous reviewers for their contribution to the peer review of this work.

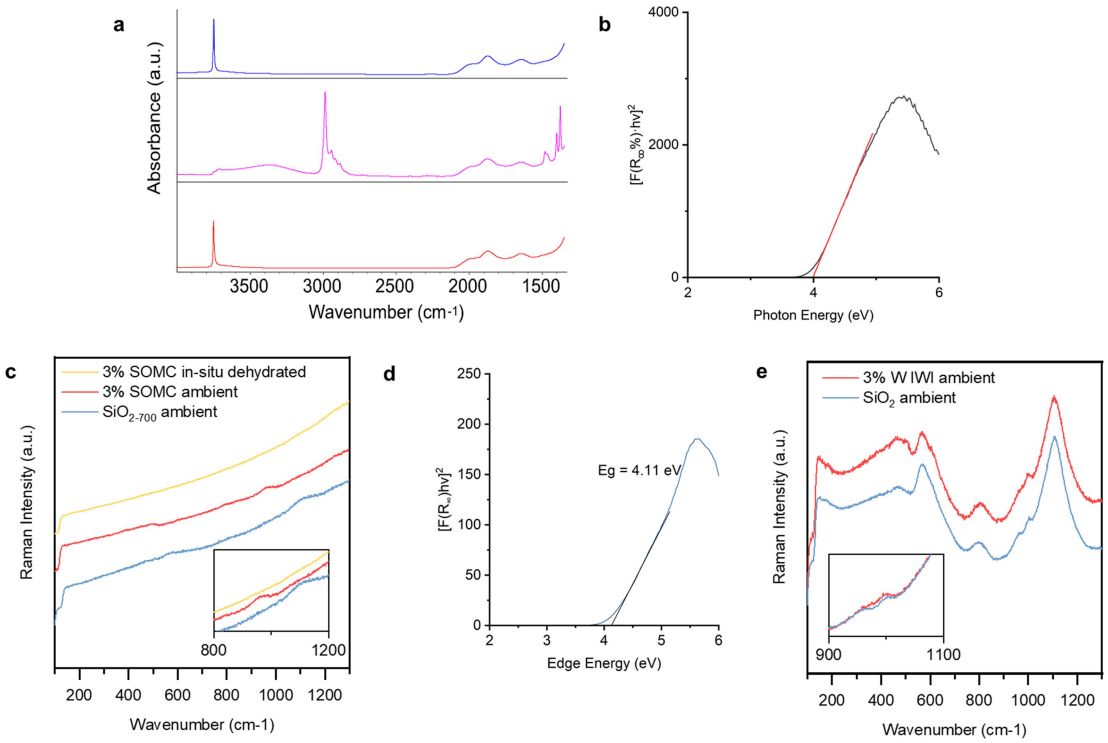

Extended Data Fig. 1 | Catalyst characterization. a, Transmission FTIR spectra of **3%SOMC** (red), grafted precursor complex (pink), and **$SiO_{2\text{-}700}$** (blue). **b**, Tauc plot of **3%SOMC**. The edge energy of 4.25 eV demonstrates that the catalyst is dominated by isolated WO_x sites[33,59]. **c**, Raman spectra of **3%SOMC** and $SiO_{2\text{-}700}$ under different environments. The in-situ dehydrated sample was heated to 450 °C (1 °C/min) for 2 h and cooled to room temperature under flowing 50 mL/min purified air. The Raman spectrum for in-situ dehydrated **3%SOMC** (yellow) was dominated by strong fluorescence, and no clear Raman features could be identified. The absence of peaks at 715 and 805 cm^{-1} in the Raman spectrum for ambient **3%SOMC** (red) indicates a lack of WO3 crystallites on the catalyst[33], and the peak at 960 cm^{-1} is attributed to WO_x under ambient conditions[33]. The peak at 1100 cm^{-1} in the $SiO_{2\text{-}700}$ spectrum (blue) is due to Si-O vibration[60]. Vertical offsets were applied for clarity. **d**, Tauc plot of 3% WO_x/SiO_2 (IWI). The edge energy of 4.11 eV demonstrates that the catalyst is dominated by isolated WO_x sites[33,59]. **e**, Raman spectra of 3% WO_x/SiO_2 IWI (3% W IWI) catalyst (red) and SiO_2 support (blue) under ambient conditions. As before, the absence of peaks at 715 and 805 cm^{-1} in the Raman spectrum indicates a lack of WO_3 crystallites on the catalyst[33]. The region from 900 to 1200 cm^{-1} is dominated by strong Raman features attributable to Si-OH (ca. 970 cm^{-1}) and Si-O vibrations (ca. 1100 cm^{-1})[60]. The subtle differences between the Raman spectra of the catalyst and support (close-up in inset) could be due to the isolated surface WO_x species on the 3% WO_x/SiO_2 IWI catalyst[33]. Vertical offsets were applied for clarity.

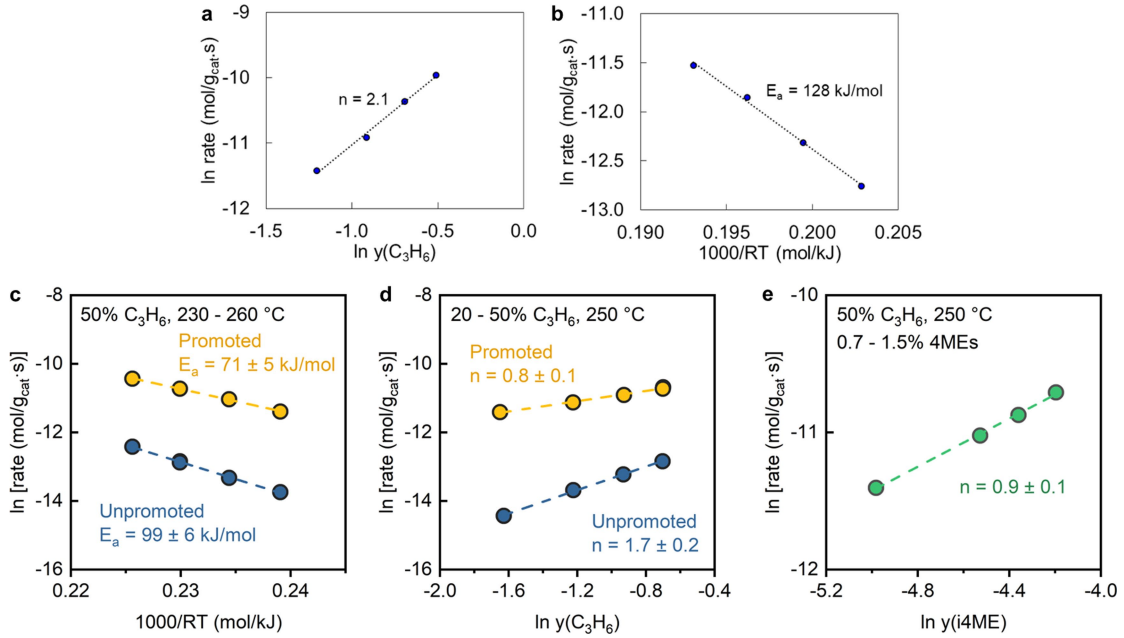

Extended Data Fig. 2 | Kinetic studies of catalysts prepared by wet impregnation. a, Reaction order plot at T = 350 °C with y(C_3H_6) = 0.3 to 0.6. **b**, Arrhenius plot at y(C_3H_6) = 0.5 with T = 320 °C to 350 °C. **c**, Arrhenius plots of propylene metathesis without promoter (blue) and with promoter (1.28 mol% 4ME + 0.22 mol% i4ME, yellow) at y(C_3H_6) = 0.5 with T = 230 °C to 260 °C. **d**, Apparent reaction order plots of propylene metathesis without promoter (blue) and with promoter (1.28 mol% 4ME + 0.22 mol% i4ME, yellow) at T = 250 °C with y(C_3H_6) = 0.2 to 0.5. **e**, Apparent reaction order plot of promoter at T = 250 °C, y(C_3H_6) = 0.5 with y(promoter) = 0.7 to 1.5 mol%. Reaction conditions: 10 mg 15% WO_x/SiO_2 (industrial) or 20 mg 3% WO_x/SiO_2 IWI, pretreated at 550 °C under 100 mL/min He for 1 h, 50 mL/min total gas flow rate (propylene + balance He or He saturated with promoter, WHSV = 0.0019 mol C_3H_6/g_{cat}.s.

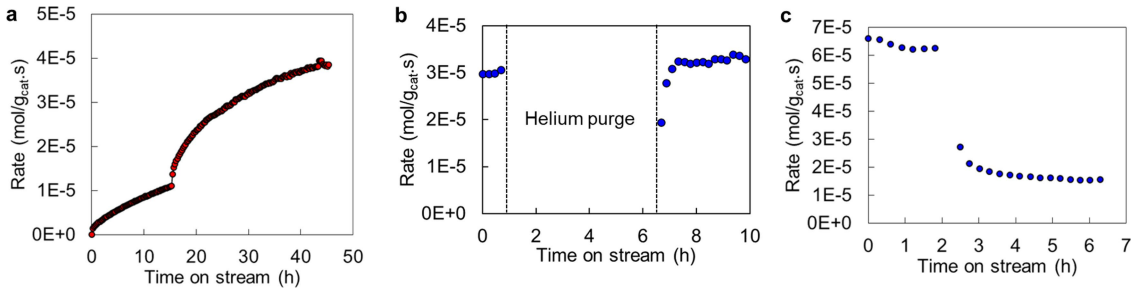

Extended Data Fig. 3 | Transient kinetic studies. a, induction period associated with **3%SOMC**. Reaction conditions: 10 mg catalyst, 25 mL/min C_3H_6 + 25 mL/min He, WHSV = 0.0019 mol C_3H_6/g_{cat}.s. The temperature was initially set to 330 °C and increased to 350 °C after ca. 15 h on stream. **b**, response of steady-state reaction to inert gas purge. TOS = 0 is defined as the time at which steady-state was originally achieved at 350 °C. Reaction conditions: 10 mg **3%SOMC**, pretreated at 550 °C under 100 mL/min He for 1 h, T = 350 °C, 50 mL/min C_3H_6 + 50 mL/min He, WHSV = 0.0037 mol C_3H_6/g_{cat}.s. **c**, response of steady-state reaction to step change in temperature. Reaction conditions: 10 mg catalyst, pretreated at 550 °C under 100 mL/min He for 1 h, 25 mL/min C_3H_6 + 25 mL/min, WHSV = 0.0019 mol C_4H_8/g_{cat}.s, The temperature was reduced from T = 330 °C to T = 300 °C between the 7th and 8th data points (the new temperature equilibrium was achieved in ca. 10 min and the 8th data point was taken after the temperature stabilized at 300 °C). TOS = 0 is defined as the point at which steady-state at 330 °C was achieved.

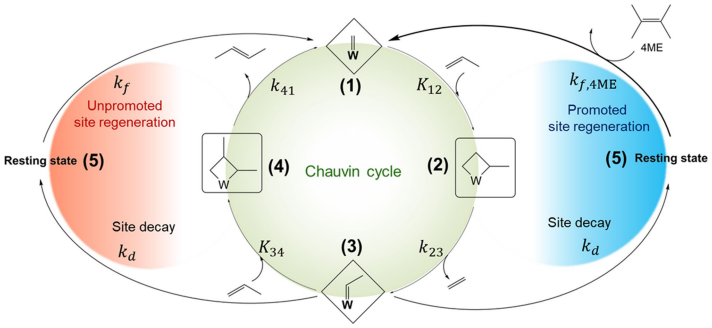

Extended Data Fig. 4 | Simplified reaction network for Chauvin metathesis including unpromoted and promoted versions of the proposed site renewal/decay cycle. The derivation of a simplified steady-state kinetic model connecting our experimental observations to our mechanistic hypotheses is presented in Methods.

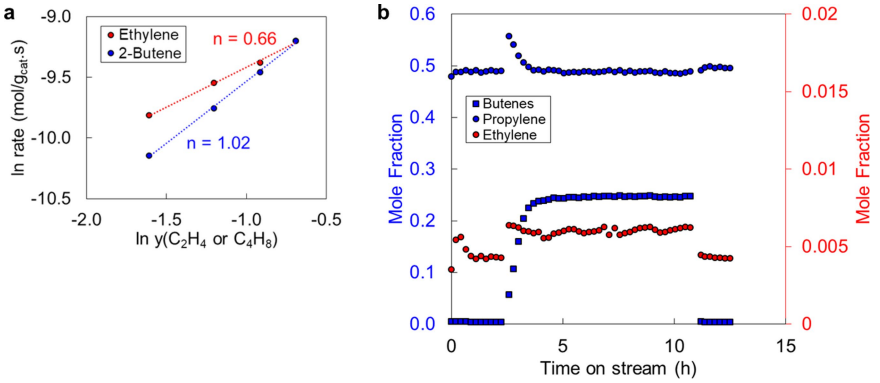

Extended Data Fig. 5 | Unusual kinetic behavior exhibited by 3%SOMC. **a**, Reaction orders for ethylene/2-butene cross-metathesis. Red: ethylene reaction order plot with $y(C_2H_4) = 0.2$ to 0.5 and $y(C_4H_8) = 0.5$. Blue: 2-butene reaction order plot with $y(C_4H_8) = 0.2$ to 0.5 and $y(C_2H_4) = 0.5$. Reaction conditions: 10 mg catalyst, pretreated at 550 °C under 100 mL/min He for 1 h, 100 mL/min total gas flow rate (balance He), WHSV = 0.0038 mol C_4H_8/g_{cat}.s, T = 330 °C. **b**, Effect of adding 2-butene to a propylene self-metathesis reaction at steady-state. The increase in ethylene yield is modest (ca. 1.5x with 20% 2-butene co-feed) but significant, stable and fully reversible, consistent with observations for better promoters such as i4ME as discussed in the text. There are two possible alternative sources of additional ethylene production upon 2-butene addition that can both be eliminated as they are too small to account for the magnitude of the increase in ethylene yield. Firstly, traces of ethylene impurities (ca. 30 ppm determined by GC-FID on a bypass run) present in the 2-butene source are 2-3 orders of magnitude too small. Secondly, 1-butene, whether as a feed impurity or generated *in situ* by isomerization, can undergo cross-metathesis with propylene to yield a 1:1 ratio of pentenes and ethylene. However, the mole fraction of pentenes in the product stream is 0.0002, an order of magnitude too small. Reaction conditions: 10 mg catalyst, pretreated at 550 °C under 100 mL/min He for 1 h, 25 mL/min C_3H_6 + 25 mL/min He or (15 mL/min He + 10 mL/min C_4H_8), WHSV = 0.0019 mol C_4H_8/g_{cat}.s, T = 330 °C.

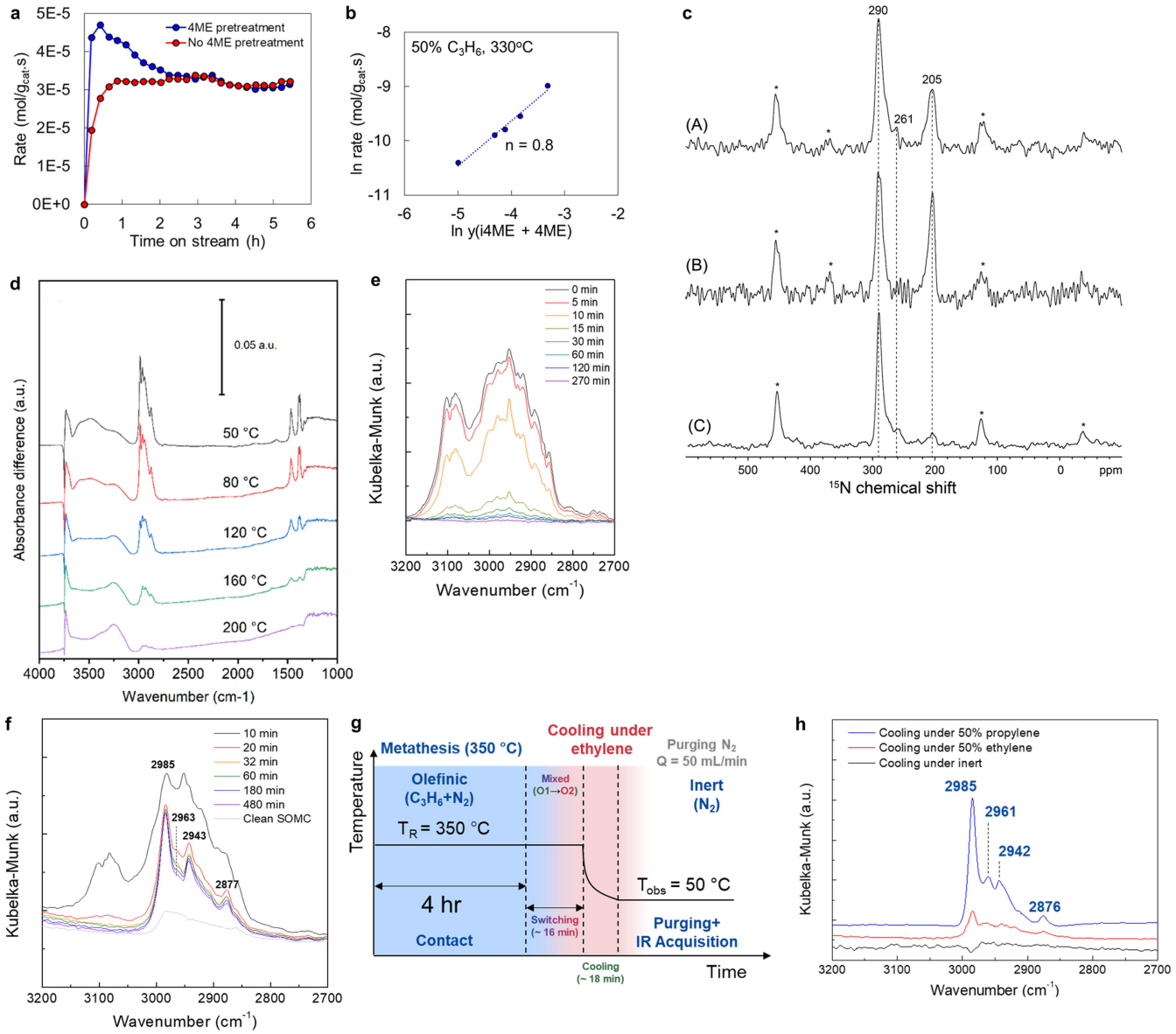

Extended Data Fig. 6 | See next page for caption.

Extended Data Fig. 6 | Mechanistic studies and control experiments. **a**, Transient behavior of purged catalyst surface pre-activated with 4ME. The initial spike in activity suggests a promotional effect of residual, adsorbed 4ME in the absence of gas-phase 4ME. A steady-state catalyst surface was first purged under helium at 350 °C for at least 3 h to destroy all active sites, then contacted with 1.5% 4ME (bal. He) for 1 h before resuming propylene flow. Reaction conditions: 10 mg catalyst, pretreated at 550 °C under 100 mL/min He for 1 h, T = 350 °C, 50 mL/min C_3H_6 + 50 mL/min He/4ME (corresponding to y_{4ME} = 0.015), WHSV = 0.0037 mol C_3H_6/g_{cat}.s. **b**, Reaction order of promoter in propylene self-metathesis. The reaction conditions are the same as in Figs. 1b and c. The promoter concentration was varied by adjusting the flow rate of promoter-saturated He (10 to 25 mL/min) and co-feeding additional He to keep the total flow rate constant. **c**, Solid-state 1D $^{15}N\{^1H\}$ CP-MAS NMR spectra of (A) **3%SOMC**, (B) **1.5%MoSOMC**, and (C) a 3 wt% WO_3/SiO_2 catalyst prepared by incipient wetness impregnation (IWI) after exposure to ^{15}N-labelled pyridine and subsequent evacuation (see Methods for details). All materials show ^{15}N NMR signals at 290 ppm and 205 ppm, which are assigned on the basis of previous computational work[61] to H-bonded ^{15}N-pyridine and ^{15}N-pyridinium, respectively, clearly establishing the presence of strong Brønsted acid sites of sufficient acidity to protonate pyridine. Additionally, both tungsten catalysts exhibit a weaker secondary signal at 261 ppm likely arising from ^{15}N-pyridine coordinated to irreducible mono-oxo W sites[12,22]. The weaker intensity of the 205 ppm peak for the IWI material (C) as compared to that of the SOMC material (A) points to a lower concentration of Brønsted acid sites that is consistent with the lower observed promotional factor. The spectra were acquired at 14.1 T, 100 K, 10 kHz MAS, with ^{15}N-^1H contact times of 3 ms. **d**, Thermal stability of surface intermediates from the low temperature chemisorption of propylene on **3%SOMC**. The temperature was ramped from 50 °C to 200 °C (5 °C/min) under flowing 50 mL/min He and held at each labeled temperature until steady state was attained. Most of the surface intermediates were desorbed below 200 °C. Vertical offsets were applied for clarity. **e**–**f**, Propylene chemisorption on pure silica (**$SiO_{2\text{-}700}$**, **e**) and pristine **3%SOMC** (**f**). We performed two control experiments to support our claim that propylene chemisorption occurs on silanols proximal to tungsten sites. Firstly, **$SiO_{2\text{-}700}$** was exposed to 50 mL/min of 50% propylene in N_2 for 4 h at 50 °C, and no visible propylene absorbance was observed after 4 h of N_2 purging (**e**). This result confirms that free surface silanols are not sufficiently acidic for reaction with propylene in the absence of tungsten sites. Next, the same chemisorption experiment was performed on pristine **3%SOMC**, omitting the high-temperature pretreatment step. As characterized in prior work[12], the isolated, coordinatively saturated tungsten sites on pristine **3%SOMC** should not undergo inner-sphere reactions with propylene at 50 °C. Observation of a spectrum virtually identical to that from propylene chemisorption on spent catalyst (**f**) thus confirms that propylene chemisorption does not directly involve the tungsten sites. **g**–**h**, DRIFTS spectra of surface intermediates arising from high temperature propylene exposure. Spent **3%SOMC** was heated to 350 °C and exposed to 50% propylene for 4 h, followed by a gas switch and rapid cooling to 50 °C under the coolant gas (**g**). Cooling under propylene (**h**, blue) resulted in the most intense absorptions derived in large proportion from low temperature chemisorption during the cooling step. Ethylene (**h**, red) does not chemisorb but appears to preserve surface intermediates, resulting in greatly attenuated peaks. The similarity of the ethylene-cooled spectrum (red) to the propylene-cooled (blue) and propylene-chemisorbed (Fig. 3a) spectra suggests that the chemisorbed species remain the dominant surface intermediates during 350 °C reaction. N_2 (**h**, black) completely destroyed all surface intermediates during the cooling step. The spectra were obtained using the clean activated **3%SOMC** background. Vertical offsets were applied for clarity.

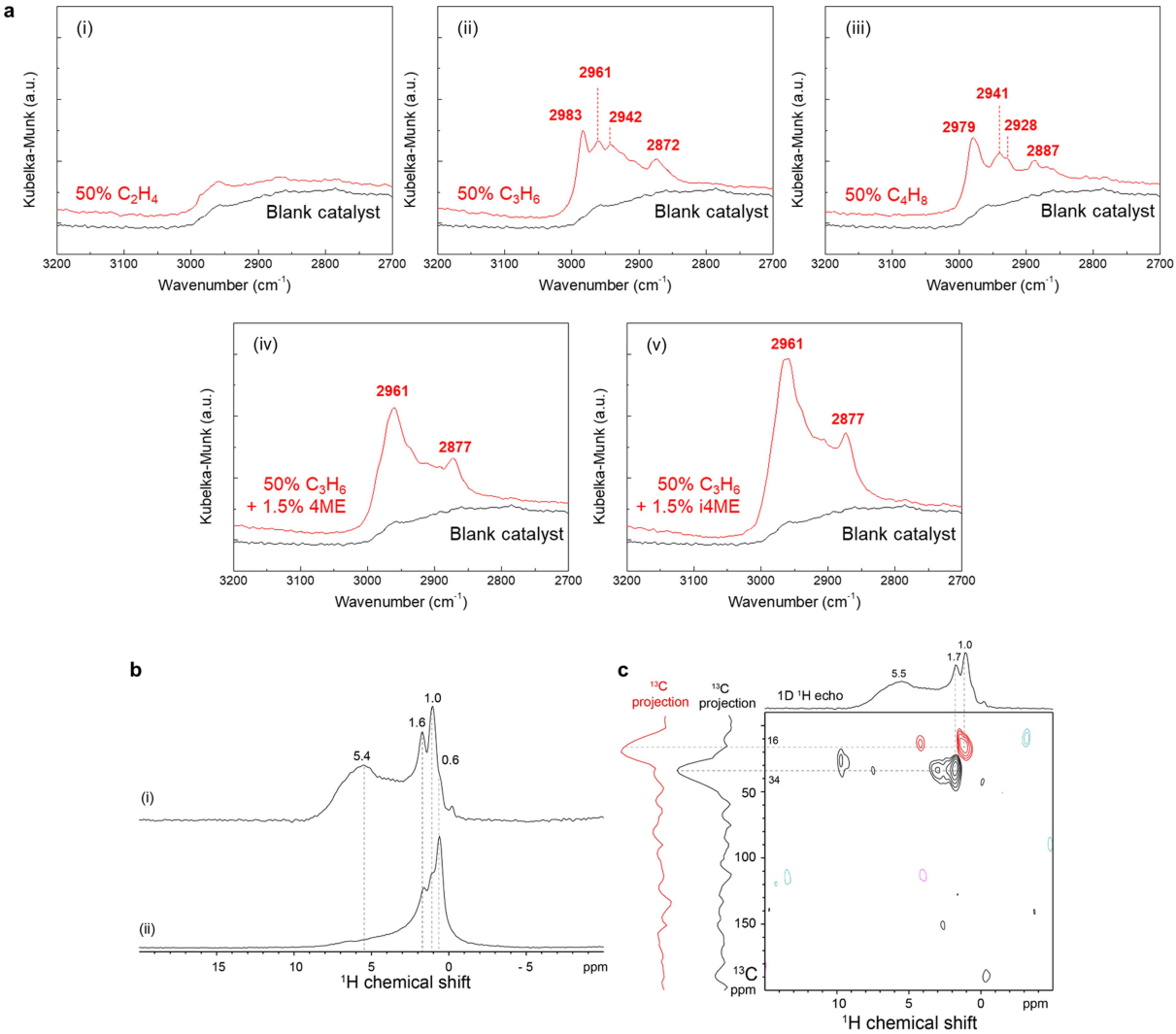

Extended Data Fig. 7 | Additional DRIFTS and solid-state NMR analysis. **a**, Low temperature chemisorption of various olefins on spent **3%SOMC**: (i) ethylene, (ii) propylene (presented in the main text but reproduced here for ease of comparison), (iii) 2-butene, (iv) propylene + 4ME, (v) propylene + i4ME. The spectrum of an activated blank catalyst (black) was obtained with respect to the KBr background. Vertical offsets were applied for clarity. Isobutene was omitted from the series because it oligomerized into a non-volatile oily phase. The fact that the peaks in (iv) and (v) (4ME and i4ME) differ only in intensity but not position is consistent with a common chemisorbed species but different thermodynamics of protonation. **b**, Solid-state 2D $^{1}H\{^{13}C\}$ D-HMQC NMR correlation spectra of **3%SOMC** reacted with propylene without i4ME. The spectra were acquired at 9.4 T, 298 K, 40 kHz MAS, and with dipolar recoupling periods of 18 rotor periods (0.45 ms, red) or 60 rotor periods (1.5 ms, black). The 1D ^{13}C projections of the two 2D spectra are shown along the ordinate, and a 1D ^{1}H echo spectrum acquired under the same conditions is shown for comparison. The short (red) and long (black) recoupling times appear to select for $-CH_3$ and $-CH_2-$ signals respectively, and the overall signals are consistent with predominantly alkyl species. Notably, the alkoxide signals of Fig. 3b are absent, likely below the detection limit of solid-state NMR. **c**, Comparison of the solid-state 1D ^{1}H MAS NMR spectra of **3%SOMC** after reaction with (top) propylene without i4ME or (bottom) propylene with i4ME. The signals are generally similar but with very different relative intensities indicating different distributions of the corresponding surface species. Specifically, reaction with propylene alone appears to result in larger relative quantities of surface-bound aromatic and/or olefinic species (^{1}H signals from 4.5–8 ppm), while reaction with i4ME appears to favor greater relative proportions of surface alkoxide and alkyl moieties. The spectra were acquired at 9.4 T, 298 K, 40 kHz MAS, and with rotor synchronized echo delays rotor periods of 2 rotor periods (0.05 ms).

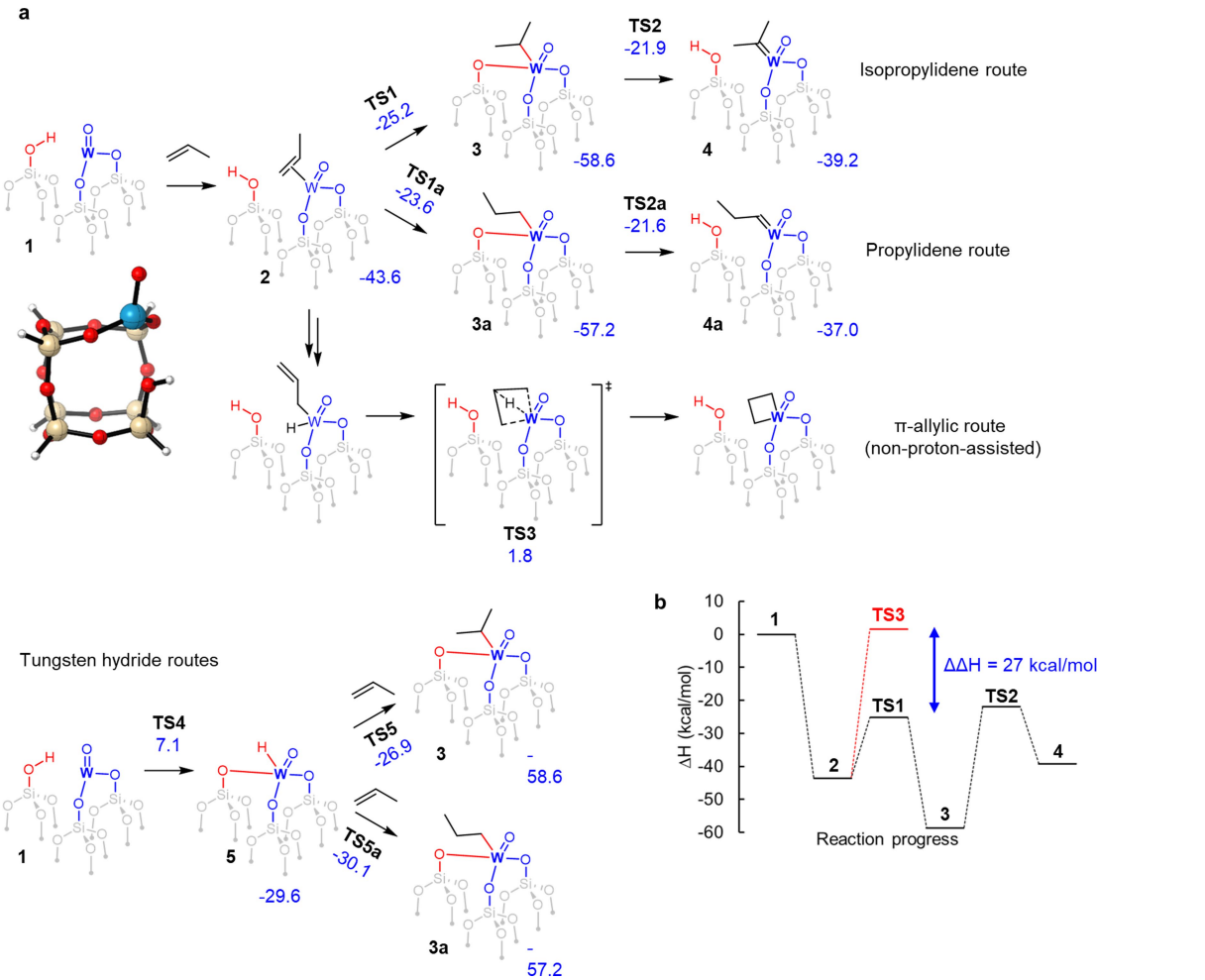

Extended Data Fig. 8 | Putative alkylidene formation pathways and preliminary computational studies. a, Proton-assisted and non-proton-assisted pathways investigated. Each structure is labeled with its 350 °C enthalpy in kcal/mol relative to infinitely separated **1** and propylene. The ball-and-stick model is an illustration of the minimal cluster model used in the computations. Full computational details are provided in Methods. **b**, Comparison of the silanol-assisted and non-silanol-assisted pathways suggests that the presence of proximal silanol groups may help to facilitate restoration of the catalytically active sites.

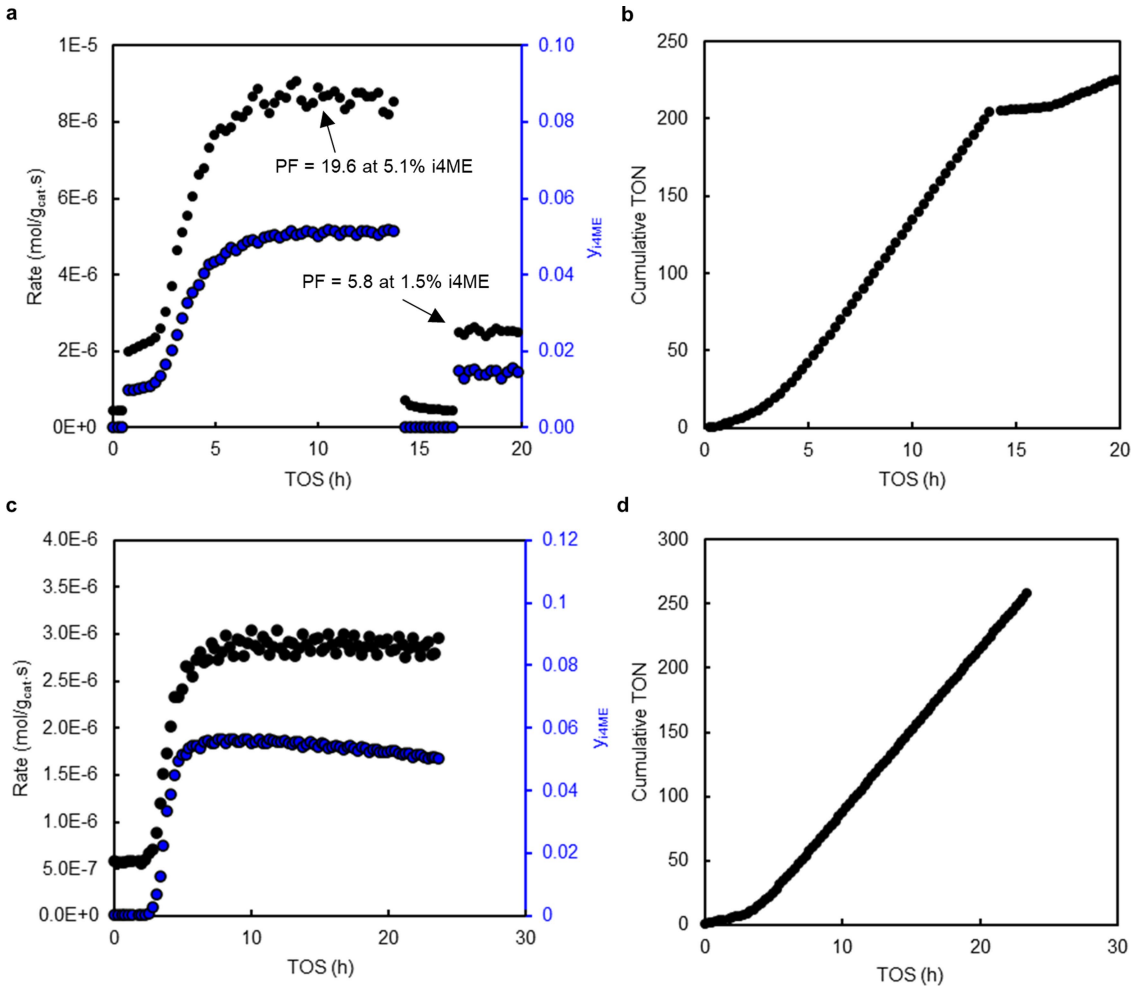

Extended Data Fig. 9 | Promotion of industrial catalyst. a, The extent of promotion of the industrial 15% WO_x/SiO_2 catalyst is lower than for **3%SOMC** (ca. 30 at 1.5% 4ME). **b**, The promotion is stable over at least several hundred turnovers (calculated based on the nominal tungsten loading, which likely overestimates the actual active site count by 1-2 orders of magnitude). Reaction conditions: 50 mg catalyst, pretreated at 550 °C under 100 mL/min He for 1 h, T = 250 °C, 25 mL/min C_3H_6 + 25 mL/min He/4ME, WHSV = 0.0019 mol C_3H_6/g_{cat}.s. Prior to promoter introduction, the catalyst was allowed to reach steady-state under 50 mL/min of 50% C_3H_6 (bal. He) at 350 °C (not shown), then cooled down to 250 °C and allowed to reach steady-state again. The zero value of time on stream (TOS) is defined to be the time at which steady-state at 250 °C was attained. **c**, i4ME promotion of industrial 15% WO_x/SiO_2 catalyst for cross-metathesis showing a lower promotion factor for cross-metathesis (ca. 5 at 5% i4ME) than for self-metathesis (ca. 20 at 5% i4ME) due to the intrinsic promotional ability of 2-butene as one of the reactants. **d**, Cross-metathesis promotion is also stable over at least several hundred turnovers. As in **b**, the turnover number is calculated based on the nominal tungsten loading. Reaction conditions: 50 mg catalyst, pretreated at 650 °C under 100 mL/min He for 1 h, T = 250 °C, 40 mL/min C_2H_4/i4ME + 10 mL/min C_4H_8. The same catalyst bed was used across panels **a**–**d**.

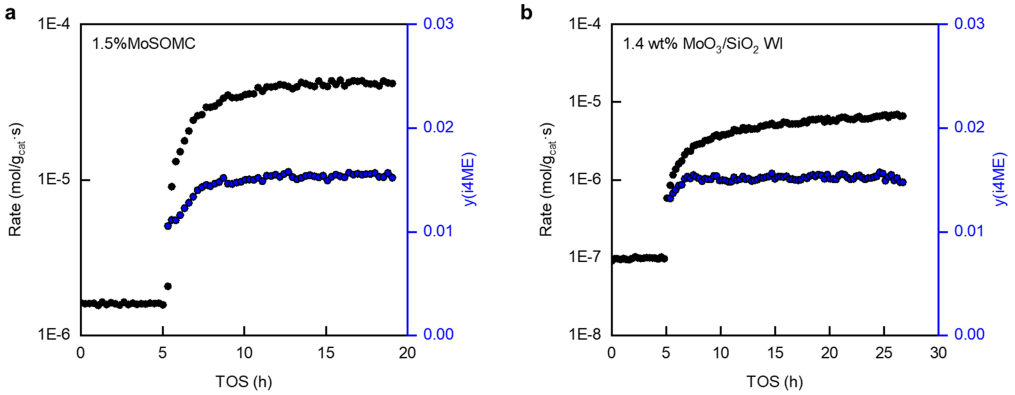

Extended Data Fig. 10 | Promotion of molybdenum-based catalysts. **a**, The promotion factor for propylene self-metathesis (ca. 26 at 1.5% i4ME) at 200 °C over **1.5%MoSOMC** catalyst. **b**, The promotion factor for propylene self-metathesis (ca. 68 at 1.5% i4ME) at 200 °C over 1.4 wt% MoO_3/SiO_2 WI catalyst. Reaction conditions: 20 mg catalyst, calcined at 400 °C under 40 mL/min air for 3 h and pretreated at 500 °C under 100 mL/min He for 3 h, T = 200 °C, 50% propylene with indicated percent of i4ME in helium balance, 50 mL/min total flow rate.

Extended Data Table 1 | Gas-chromatography characterization of reaction products

a

Retention time (min)	Identification	Unpromoted		Promoted	
		Peak area	Mole fraction	Peak area	Mole fraction
2.1	Ethylene	18531	1.55×10^{-4}	546219	4.55×10^{-3}
2.4	Propane (propylene impurity)	262288	1.47×10^{-3}	265276	1.49×10^{-3}
3.1	Propylene	88745859	0.499	88343707	0.497
5.6	2-butene (trans)	17005	7.55×10^{-5}	490864	2.18×10^{-3}
6.1	Isobutene	-	-	10925	4.85×10^{-5}
6.3	2-butene (cis)	18506	8.22×10^{-5}	525300	2.33×10^{-3}
8.4	3ME	-	-	6491	2.32×10^{-5}
10.0	i4ME/4ME*	-	-	5250262	0.0158
12.0	Unidentified $>C_6$ products	-	-	5205	1.35×10^{-5}

b

S/N	Catalyst	Feed	i4ME:4ME ratio in effluent
1	SiO_2	50% C_3H_6 + 1.5% i4ME	74:1
2	**3%SOMC**	50% C_3H_6 + 1.5% i4ME	1.1:1
3	**3%SOMC**	50% C_3H_6 + 1.5% 4ME	0.3:1

a, Identification and quantification of unpromoted and promoted propylene self-metathesis products. * as noted in Methods, these two peaks could not be separated. Rate of metathesis product (ethylene + 2-butene) formation with promoter = 2.25×10^{-5} mol/g_{cat}.s. Rate of side product (isobutene + 3ME + $>C_6$) formation = 2.11×10^{-7} mol/g_{cat}.s. Side product selectivity = 0.0094. Peak areas presented are averaged over 5 consecutive injections at steady-state, and mole fractions computed from pre-determined calibration factors (see Methods for details). Reaction conditions are the same as in Fig. 2. Note that 1-butene, a by-product sometimes seen in propylene metathesis, was not produced in significant amounts in either run (FID peak area < 1000). **b**, Interconversion of 4ME and i4ME under reaction conditions. Pure silica does not isomerize i4ME to any significant extent even at elevated temperatures. Interestingly, the extent of isomerization in either direction does not approach that predicted by thermodynamic equilibrium, which would be <0.01:1 in favor of 4ME. This suggests that, as we postulate in the main text, a steady-state i4ME:4ME ratio can be achieved by separating and recycling the promoter in the effluent. Reaction conditions: 10 mg **3%SOMC** (S/N 2 and 3), pretreated at 550 °C under 100 mL/min He for 1h, 25 mL/min C_3H_6 + 25 mL/min He saturated with promoter, WHSV = 0.0019 mol C_4H_8/g_{cat}.s, T = 280 °C. It should also be noted that the BASF R3-11G catalyst used for feed purification (see Methods for more information) can also catalyse isomerization of i4ME/4ME at room temperature, and the usage of excessive quantities may result in deviations from the values in the table.

Extended Data Table 2 | Physical parameters used to evaluate heat and mass transfer limitations

Physical quantity	Symbol	Value (1 s.f.)	Notes
Catalyst particle radius	r_p	2×10^{-4} m	Assuming 40 mesh and spherical
Average pore diameter for catalyst particles	d_p	2.5×10^{-8} m	
Bulk propylene concentration	C_A	10 mol/m^3	From ideal gas law
Tubing inner radius	r_t	2×10^{-3} m	
Total gas flow rate	Q	2×10^{-6} m^3/s	Converted from STP to reaction T
Density of gas mixture	r	0.4 kg/m^3	From ideal gas law assuming equimolar He and propylene mixture
Viscosity of gas mixture	m	3×10^{-5} Pa.s	Estimated from arithmetic mean of pure helium and propylene viscosities
Reynolds number	Re	8	
Schmidt number	Sc	0.8	
Bulk gas diffusivity	D_{AB}	1×10^{-4} m/s	Typical value for ideal gas mixtures
Mass transfer coefficient	k_m	0.1 m/s	$Sh = k_m(2r_p)/D_{AB} = 2 + Re^{1/2}Sc^{1/3}$ for laminar flow over a sphere
Mean velocity	ν	537 m/s	$[(8k_BT)/(\pi m)]^{1/2}$
Knudsen diffusivity	D_K	5×10^{-6} m^2/s	$\nu d_p/3$
Effective diffusivity	D_e	4×10^{-6} m^2/s	$D_e = 1/(1/D_b+1/D_K)$
Thermal conductivity of gas mixture	k_g	0.1 W/m.K	
Heat capacity of gas mixture	C_p	2×10^3 J/kg.K	Weighted average of pure helium and propylene heat capacities
Prandtl number	Pr	0.6	
Heat transfer coefficient	h	1×10^3 W/m^2.K	$Nu = h(2r_p)/k_g = 2 + Re^{1/2}Pr^{1/3}$ for laminar flow over a sphere
Density of catalyst support	r_s	1×10^3 kg/m^3	Approximated as density of crystalline silica multiplied by porosity of 0.4
Observed reaction rate (volumetric)	r'''	80 mol/m$^3_{cat}$.s	From $r = 1 \times 10^{-4}$ mol/g$_{cat}$.s
Thermal conductivity of support	k	1 W/m.K	
Reaction enthalpy	ΔH_r	6 kJ/mol	
Apparent activation energy	E_a	200 kJ/mol	

The source of each parameter is indicated in the rightmost column, and the application of the Weisz–Prater and Mears criteria is as shown in Methods (Kinetic studies).